

**INVESTIGATION OF ATMOSPHERIC OZONE
IMPACTS OF METHYL IODIDE**

Final Report to the

Arysta LifeScience Corporation
Contract UCR-07041867

By

William P. L. Carter

July 31, 2007

Center for Environmental Research and Technology
College of Engineering
University of California
Riverside, California 92521

ABSTRACT

An experimental and modeling study was carried out to assess the impacts of methyl iodide on ground-level ozone formation compared to other chemicals that are emitted into the atmosphere. The experiments consisted of environmental chamber irradiations of methyl iodide and NO_x with and without added CO, methyl iodide and O_3 with CO, and incremental reactivity environmental chamber experiments to determine the effect of adding methyl iodide to irradiations of reactive organic gas (ROG) surrogate - NO_x mixtures representing ambient conditions. The results were modeled using the SAPRC-07 mechanism with the reactions of methyl iodide and iodine species added. The data were reasonably well simulated after adjusting uncertain parameters concerning photolysis rate of INO_2 and the formation of I_xO_x oligomers from the reactions of IO radicals. This mechanism was then used to calculate the atmospheric impact of methyl iodide in the box model scenarios to derive the Maximum Incremental Reactivity (MIR) and other reactivity scales. Methyl iodide was calculated to inhibit ozone under all conditions except those with very high NO_x levels, where its impact is comparable to that for ethane. It is concluded that methyl iodide should not be regulated as contributing to ground level ozone formation.

ACKNOWLEDGEMENTS AND DISCLAIMERS

This work was funded by the Arysta LifeScience Corporation through contract number UCR-07041867. The environmental chamber experiments for this project were carried out at the College of Engineering Center for Environmental Research and Technology (CE-CERT) primarily by Kurt Bumiller, Qi Li., Quentin Malloy and Bethany Warren. Mr. Dennis Fitz also provided assistance in administering this project.

Although this work was funded by Arysta LifeScience Corporation, the contents of this report reflect only the opinions and conclusions of the author. Mention of trade names and commercial products does not constitute endorsement or recommendation for use.

TABLE OF CONTENTS

INTRODUCTION	1
EXPERIMENTAL METHODS	3
Chamber Description.....	3
Analytical Instrumentation	5
Sampling methods	8
Characterization Methods.....	8
Experimental Procedures.....	9
Materials.....	10
MECHANISM AND MODELING METHODS	11
Base Mechanism.....	11
Methyl Iodide Mechanism and Reactions of Iodine Species	12
Representation of Chamber Conditions.....	17
Atmospheric Reactivity Simulations	18
RESULTS AND DISCUSSION	19
Characterization Results	19
Light Characterization	19
Chamber Effects Characterization	22
Mechanism Evaluation Results	23
Atmospheric Reactivity Calculations	29
CONCLUSIONS.....	35
REFERENCES	37
APPENDIX A. BASE MECHANISM LISTING	40

LIST OF TABLES

Table 1.	Summary of compounds in a current California pesticide VOC emissions inventory and their ozone impacts in the MIR scale.	1
Table 2.	List of analytical and characterization instrumentation for the UCR EPA chamber.	6
Table 3.	Mechanism for methyl iodide used in this work.	13
Table 4.	Absorption cross-sections used for the photolysis reactions in the methyl iodide mechanism.	15
Table 5.	Summary of experiments carried out for this project.	20
Table 6.	Summary of initial concentrations and selected results for the methyl iodide - NO _x , methyl iodide - CO - NO _x , and methyl iodide - O ₃ - CO irradiations.	24
Table 7.	Summary of initial concentrations and selected gas-phase results of the incremental reactivity experiments.	27
Table 8.	Summary of conditions of scenarios used for reactivity assessment.	30
Table 9.	Calculated atmospheric incremental reactivities for methyl iodide and ethane.	32
Table A-1.	List of model species used in the base SAPRC-07 mechanism, including the VOC species used in the chamber and atmospheric reactivity simulations.	40
Table A-2.	Reactions and rate constants in the base SAPRC-07 mechanism used in this work. See Carter (2007) for documentation.	44
Table A-3.	Summary of photolysis rates used in chamber and ambient simulations. Absorption cross sections and quantum yields used to calculate these photolysis rates are given by Carter (2007) for reactions in the base mechanism and in Table 4 for those in the methyl iodide mechanism.	60

LIST OF FIGURES

Figure 1.	Schematic of the UCR EPA environmental chamber reactors and enclosure.	4
Figure 2.	Spectrum of the argon arc light source used in the UCR EPA chamber. Blacklight and representative solar spectra, with relative intensities normalized to give the same NO ₂ photolysis rate as that for the UCR EPA spectrum, are also shown.	4
Figure 3.	Plots of light intensity data used to assign NO ₂ photolysis rates for the blacklight light source.	21
Figure 4.	Plots of best fit HONO offgasing parameters against UCR EPA run number.).....	22
Figure 5.	Experimental and calculated results of the methyl iodide - NO _x experiments.	24
Figure 6.	Experimental and calculated results of the methyl iodide + CO - NO _x experiments.	25
Figure 7.	Experimental and calculated results of O ₃ - CO and O ₃ - CO - Methyl iodide irradiation experiments.	25
Figure 8.	Experimental and calculated results of the incremental reactivity experiments with added methyl iodide.	28
Figure 9.	Plots of incremental reactivities of methyl iodide in the atmospheric reactivity scenarios against the ROG / NO _x input ratio.....	33
Figure 10.	Plots of incremental reactivities of methyl iodide and ethane in the atmospheric reactivity scenarios against the ROG/NO _x ratio, normalized by the ROG/NO _x ratio yielding the maximum ozone concentrations.....	33

INTRODUCTION

Methyl iodide (CH₃I) is being proposed as a potential replacement for methyl bromide because of its shorter atmospheric lifetime and thus lower impact on stratospheric ozone and global warming. However, while the shorter atmospheric lifetime is an advantage with regard to global impacts, its reactions on a local or regional scale may promote the formation of ground-level ozone, a serious air quality problem in many areas. Ground level ozone is not emitted directly; it is formed from the gas-phase atmospheric reactions of emitted volatile organic compounds (VOCs) in the presence of oxides of nitrogen (NO_x) in air. Methyl iodide is an example of a VOC whose reactions could affect ozone formation.

Not all VOCs are equal in their impact on ground-level ozone. The impact on ozone formation depends on how rapidly the VOC reacts and the amount of ozone formed once the VOC reacts. Methyl bromide reacts in the lower atmosphere relatively slowly, and thus its impact on ground level ozone formation is very low (Carter, 2007). On the other hand, because of its relatively rapid photolysis under atmospheric conditions, with a half life of about 1-2 days, methyl iodide may have a non-negligible impact on ozone formation. In addition, as discussed below the photolysis reaction is expected to form radicals whose subsequent reactions may be highly effective in promoting ozone formation. However, at present there are no estimates available concerning the quantitative impacts of methyl iodide on ozone formation under atmospheric conditions.

Because of the complexity of the environmental and chemical factors involved in ground-level ozone formation (e.g., NRC, 1991), the only practical method to make quantitative estimates of ozone impacts of VOCs is to develop a gas-phase atmospheric reaction mechanism for the compound, evaluate and verify its predictions of ozone impacts by using appropriate environmental chamber data with the compound, then use the mechanism in computer airshed models of various regions to calculate the changes in ozone formation caused by adding the particular compound to the emissions. Examples of the development and evaluation of mechanisms for predicting impacts of individual VOCs is given by Carter (2000a, 2007), and examples of using such mechanisms for deriving ozone reactivity scales quantifying the impacts of the VOCs on ozone formation under various conditions is given by Carter (1994a). An updated version of the Maximum Incremental Reactivity (MIR) scale of Carter (1994a) has been utilized in California's ozone reactivity-based regulations for alternatively-fueled vehicles (CARB, 1993) and aerosol coatings (CARB, 2000) and is being considered for other applications as well. This scale has recently been updated again based on information current as of 2007 (Carter, 2007). MIR's for compounds in current California emissions inventories for pesticide use are shown in Table 1.

Unfortunately, there are significant uncertainties concerning the reactions of the iodine species expected to be formed when methyl iodide reacts, and there are no experimental data available concerning the impact of methyl iodide on ozone formation under atmospheric conditions. Although as one could derive estimated mechanisms for the atmospheric reactions of iodine species (e.g., see Jimenez et al, 2003), because of the uncertainties in their mechanisms any estimates of atmospheric ozone impact calculations using these mechanisms would be so unreliable as to be unsuitable for regulatory or environmental assessment planning. At a minimum, the predictive capabilities of the mechanisms for methyl iodide would need to be evaluated by comparing its predictions against results of appropriate environmental chamber experiments with the compound, as has been done for most of the major types of VOCs that have been emitted (Carter, 2007 and references therein). Even though the estimated mechanism may still have uncertainties, if its predictions are consistent with the results of experiments

Table 1. Summary of compounds in a current California pesticide VOC emissions inventory and their ozone impacts in the MIR scale.

Compound or Mixture	Mass fract. [a]	V.P. (ppm) [b]	MIR [c]	Comment
Methyl bromide	25.3%	High	~0.02	Approximate mechanism
Methyl isothiocyanate	17.8%	High	0.31	
1,3-Dichloropropenes	11.3%	High	4.30	
Chloropicrin	8.6%	High	1.88	
Aromatic 200 solvent	4.8%	High	~3 - 7	Depends on composition.
Xylene range solvent	4.6%	High	~7.8	Based on representative xylene mixture
Molinate	3.3%	7.4	1.44	
Kerosene	1.7%	Moderate	1.47	
Chlorpyrifos	1.7%	0.03		Low volatility
Methylisobutyl ketone	0.8%	High	3.83	
Glyphosate, isopropylamine salt	0.7%	Low		Not volatile
Acrolein	0.7%	High	7.42	
Glycerine	0.5%	0.22	3.11	
Propylene glycol	0.5%	170	2.53	
Thiobencarb	0.5%	0.03	0.65	
N-Methyl pyrrolidinone	0.5%	454	2.30	
S-ethyl N,N-dipropyl thiocarbamate	0.5%	32	1.59	
Oxyfluorfen	0.5%	0.0003		Low volatility
Pebulate	0.4%	116	1.60	
Pendimethalin	0.4%	0.04		Low volatility
Oryzalin	0.3%	0.00001		Not volatile
Trifluralin	0.2%	0.06		Low volatility
Aliphatic solvent	0.2%	High		Depends on composition
Oxydemeton-methyl	0.2%	0.04		Low volatility
Representative non-pesticide VOCs (shown for comparison purposes)				
Mixture used to represent VOC emissions from all sources	-	High	3.60	Compounds with higher MIR have higher ozone impact than average
Ethane	-	High	0.27	Used by the EPA as the standard to define "negligible" reactivity (Dimitriades, 1999)

[a] Mass Fraction of compound in total pesticide VOC profile used in California emissions inventories. Data provided by the CARB staff in October, 2004. The unidentified fraction is not shown.

[b] Vapor pressures at 25oC obtained from the Syracuse Research Corporation (SRC) online physical properties database at <http://www.syrres.com/esc/physdemo.htm>. "High" means that the vapor pressure is greater than 1000 ppm. "Low" means probably has negligible volatility.

[c] Calculated ozone reactivity in grams O₃ per gram VOC in the MIR scale as given by Carter (2007). See Carter (2007) for a summary of the experiments used to evaluate the mechanisms for these compounds.

representing a sufficiently varied set of conditions then the uncertainty range of the atmospheric ozone predictions would be significantly reduced.

In view of this, Arysta LifeScience Corporation funded the College of Engineering, Center for Environmental Research and Technology (CE-CERT) at the University of California at Riverside (UCR) to carry out a project to reduce uncertainties in estimates of the atmospheric ozone impacts of methyl iodide. This included conducting environmental chamber experiments suitable for testing mechanisms for the gas-phase atmospheric reactions of methyl iodide that affect ozone formation, deriving mechanisms for predicting the atmospheric ozone and other impacts of methyl iodide that are consistent with the environmental chamber data, and calculating atmospheric ozone impacts of methyl iodide using the chemical mechanism so developed, and comparing these impacts with those for other VOCs. The approach used is similar to that used many other VOCs that have been studied previously (Carter, 2007, and references therein). The methods, results, and conclusions of this project are documented in this report.

EXPERIMENTAL METHODS

Chamber Description

All of the environmental chamber experiments for this project were carried out using the UCR EPA environmental chamber. This chamber was constructed under EPA funding to address the needs for an improved environmental chamber database for mechanism evaluation (Carter et al, 1999, Carter, 2002). The objectives, design, construction, and results of the initial evaluation of this chamber facility are described in more detail elsewhere (Carter et al, 1999, Carter, 2002; Carter, 2004, Carter et al, 2005a). A description of the chamber is also given below.

The UCR EPA chamber consists of two ~85,000-liter Teflon® reactors located inside a 16,000 cubic ft temperature-controlled “clean room” that is continuously flushed with purified air. The clean room design is employed in order to minimize background contaminants into the reactor due to permeation or leaks. Two alternative light sources can be used. The first consists of a 200 KW argon arc lamp with specially designed UV filters that give a UV and visible spectrum similar to sunlight. This light source could not be used for this project because it was not operational during this period. Banks of blacklights are also present to serve as a backup light source for experiments where blacklight irradiation is sufficient, and this was used for the experiments for this project because of availability and because use of blacklights was judged to be sufficient to satisfy the project objectives. The interior of the enclosure is covered with reflective aluminum panels in order to maximize the available light intensity and to attain sufficient light uniformity, which is estimated to be $\pm 10\%$ or better in the portion of the enclosure where the reactors are located (Carter, 2002). A diagram of the enclosure and reactors is shown in Figure 1, and spectra of the light sources are shown in Figure 2.

The dual reactors are constructed of flexible 2 mil Teflon® film, which is the same material used in the other UCR Teflon chambers used for mechanism evaluation (e.g., Carter et al, 1995a; Carter, 2000a, and references therein). A semi-flexible framework design was developed to minimize leakage and simplify the management of large volume reactors. The Teflon film is heat-sealed into separate sheets for the top, bottom, and sides (the latter sealed into a cylindrical shape) that are held together and in place using bottom frames attached to the floor and moveable top frames. The moveable top frame is held to the ceiling by cables that are controlled by motors that raise the top to allow the reactors to expand when filled or lower the top to allow the volume to contract when the reactors are being emptied or flushed. These motors in turn are controlled by pressure sensors that raise or lower the reactors as needed to maintain slight positive pressure. During experiments the top frames are slowly lowered to maintain continuous positive pressure as the reactor volumes decrease due to sampling or leaks. The experiment is terminated once the volume of one of the reactor reaches about 1/3 the maximum value, where the time this took varied depending on the amount of leaks in the reactor, but was greater than the duration of most of the experiments discussed in this report. Since at least some leaks are unavoidable in large Teflon film reactors, the constant positive pressure is important to minimize the introduction of enclosure air into the reactor that may otherwise result.

As indicated in Figure 1, the floor of the reactors has openings for a high volume mixing system for mixing reactants within a reactor and also for exchanging reactants between the reactors to achieve equal concentrations in each. This utilizes four 10” Teflon pipes with Teflon-coated blowers and flanges

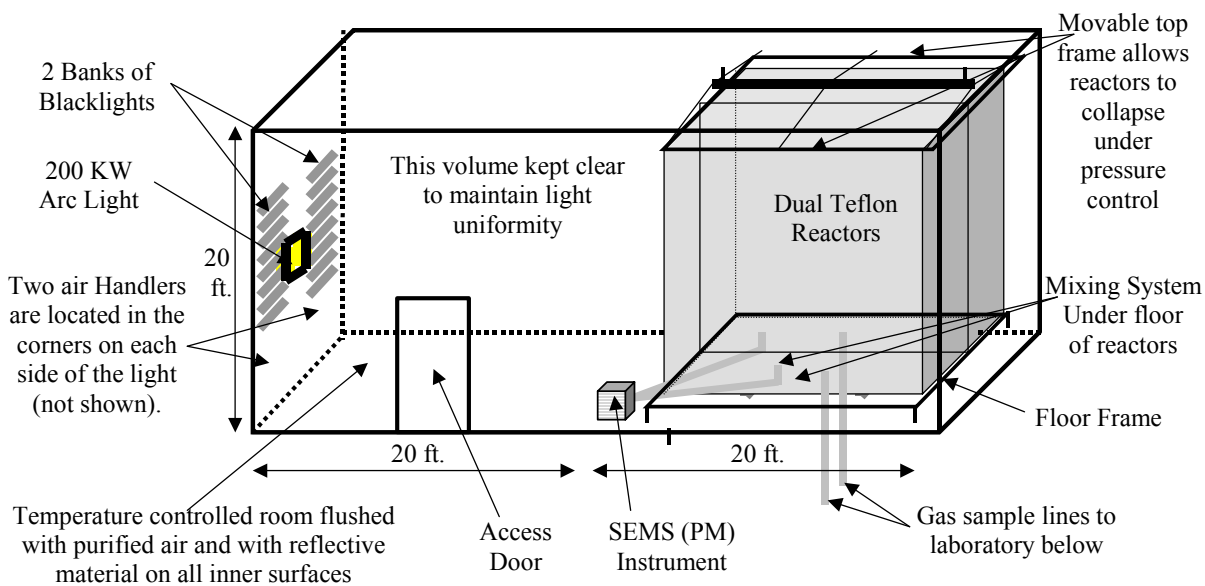


Figure 1. Schematic of the UCR EPA environmental chamber reactors and enclosure.

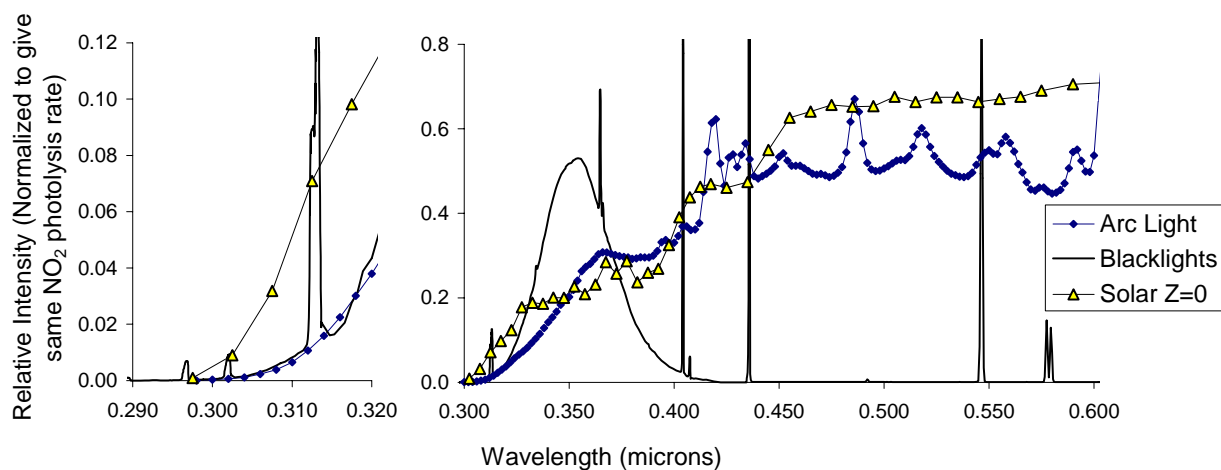


Figure 2. Spectrum of the argon arc light source used in the UCR EPA chamber. Blacklight and representative solar spectra, with relative intensities normalized to give the same NO_2 photolysis rate as that for the UCR EPA spectrum, are also shown.

to either blow air from one side of a reactor to the other, or to move air between each of the two reactors. Teflon-coated air-driven metal valves are used to close off the openings to the mixing system when not in use, and during the irradiation experiments.

An AADCO air purification system that provides dry purified air at flow rates up to 1500 liters min^{-1} is used to supply the air to flush the enclosure and to flush and fill the reactors between experiments. The air is further purified by passing it through cartridges filled with Purafil® and heated Carulite 300® which is a Hopcalite® type catalyst and also through a filter to remove particulate matter. The measured NO_x , CO, and non-methane organic concentrations in the purified air were found to be less than the detection limits of the instrumentation employed (see Analytical Equipment, below).

The chamber enclosure is located on the second floor of a two-floor laboratory building that was designed and constructed specifically to house this facility (Carter et al, 2002). Most of the analytical instrumentation is located on the ground floor beneath the chamber, with sampling lines leading down as indicated in Figure 1.

Analytical Instrumentation

Table 2 gives a listing of the analytical and characterization instrumentation whose data were utilized for this project. Other instrumentation was available and used for some of these experiments, as discussed by Carter 2002a and Carter et al, 2005a, but the data obtained were not characterized for modeling and thus not used in the mechanism evaluations for this project. The table includes a brief description of the equipment, species monitored, and their approximate sensitivities, where applicable. These are discussed further in the following sections.

Ozone, CO, NO, and NO_y were monitored using commercially available instruments as indicated in Table 2. The instruments were spanned for NO, NO_2 , and CO and zeroed prior to most experiments using the gas calibration system indicated in Table 2, and a prepared calibration gas cylinder with known amounts of NO and CO. O_3 and NO_2 spans were conducted by gas phase titration using the calibrator during this period. Span and zero corrections were made to the NO, NO_2 , and CO data as appropriate based on the results of these span measurements, and the O_3 spans indicated that the UV absorption instrument was performing within its specifications.

Organic reactants other than formaldehyde were measured by gas chromatography with FID detection as described elsewhere (Carter et al, 1995a); see also Table 2. The surrogate gaseous compounds ethylene, propylene, n-butane and trans-2-butene were monitored by using 30 m megabore GS-Alumina column and the loop sampling system. The second signal of the same GC outfitted with FID, loop sampling system and 30 m megabore DB-5 column was used to analyze surrogate liquid components toluene, n-octane and m-xylene. The sampling methods employed for injecting the sample with the test compounds on the GC column depended on the volatility or “stickiness” of the compounds. For analyses of more volatile species such as methyl iodide the same loop method was suitable.

Both the GC instruments were controlled and their data were analyzed using HPChem software installed on a dedicated PC. The GC's were spanned using the prepared calibration cylinder with known amounts of ethylene, propane, propylene, n-butane, n-hexane, toluene, n-octane and m-xylene in ultrapure nitrogen. Analyses of the span mixture were conducted approximately every day an experiment was run, and the results were tracked for consistency.

Table 2. List of analytical and characterization instrumentation for the UCR EPA chamber.

Type	Model or Description	Species	Sensitivity	Comments
Ozone Analyzer	Dasibi Model 1003-AH. UV absorption analysis. Also, a Monitor Labs Chemiluminescence Ozone Analyzer Model 8410 was used as a backup.	O ₃	2 ppb	Standard monitoring instrument.
NO - NO _y Analyzer	Teco Model 42 C with external converter. Chemiluminescent analysis for NO, NO _y by catalytic conversion.	NO NO _y	1 ppb 1 ppb	Useful for NO and initial NO ₂ monitoring. Converter close-coupled to the reactors so the “NO _y ” channel should include HNO ₃ as well as NO ₂ , PANs, organic nitrates, and other species converted to NO by the catalyst.
CO Analyzer	Thermo Environmental Instruments Inc. Model 48 C	CO	50 ppb	Standard monitoring instrument
GC-FID Instruments	Dual HP 6890 Series II GC with dual columns, loop injectors and FID detectors. Controlled by computer interfaced to network.	VOCs	~10 ppbC	30 m x 0.53 mm GS-Alumina column used for the analysis of light hydrocarbons such as ethylene, propylene, n-butane and trans-2-butene and 30 m x 0.53 mm DB-5 column used for the analysis of C ₅₊ alkanes and aromatics, such as toluene and m-xylene. Loop injection is suitable for low to medium volatility VOCs that are not too “sticky” to pass through valves. Two 30 m x 0.32 mm DB-5 column measure C ₅₊ alkanes and aromatics, such as toluene and m-xylene.
PTR-MS	Ionicon Analytik high sensitivity proton transfer reaction mass spectrometer equipped with a quadruple MS. Controlled by computer interface.	VOCs	~5ppt	Used to measure light VOCs such as formaldehyde and parent hydrocarbons. (Used primarily for formaldehyde in experiments for this project.)
Gas Calibrator	Model 146C Thermo Environmental Dynamic Gas Calibrator	N/A	N/A	Used for calibration of NO _x and other analyzers. Instrument acquired early in project and under continuous use.
Data Acquisition System	Windows PC with custom LabView software, 16 analog input, 40 I/O, 16 thermo-couple, and 8 RS-232 channels.	N/A	N/A	Used to collect data from most monitoring instruments and control sampling solenoids. In-house LabView software was developed using software developed by Sonoma Technology for ARB for the Central California Air Quality Study as the starting point.

Table 2 (continued)

Type	Model or Description	Species	Sensitivity	Comments
Temperature sensors	Various thermocouples, radiation shielded thermocouple housing	Temperature	~0.1 °C	Primary measurement is thermocouples inside reactor. However, comparison with temperature measurements in the sample line suggest that irradiative heating may bias these data high by ~2.5°C. See text.
Humidity Monitor	General Eastern HYGRO-M1 Dew Point Monitor	Humidity	Dew point range: -40 - 50°C	Instrument performs as expected, but dew point below the performance range for most of the experiments discussed in this report, except for those with added humidity.
Spectroradiometer	LiCor LI-1800 Spectroradiometer	300-850 nm Light Spectrum	Adequate	Resolution relatively low but adequate for this project. Used to obtain relative spectrum. Also gives an absolute intensity measurement on surface useful for assessing relative trends.
QSL Spherical Irradiance Sensor	Biospherical QSL-2100 PAR Irradiance Sensor. Responds to 400-700 nm light.	Spherical Broad-band Light Intensity	Adequate	Provides a measure of absolute intensity and light uniformity that is more directly related to photolysis rates than light intensity on surface. Gives more precise measurement of light intensity trends than NO ₂ actinometry, but is relatively sensitive to small changes in position.
Scanning Electrical Mobility Spectrometer (SEMS)	TSI 3080L column, TSI 3077 ⁸⁵ Kr neutralizer, and TSI 3760A CPC. Instrument design, control, and operation similar to that described in Cocker et al. (2001)	Aerosol number and size distributions	Adequate	Provides information on size distribution of aerosols in the 28-730 nm size range, which accounts for most of the aerosol mass formed in our experiments. Data can be used to assess effects of VOCs on secondary PM formation.

The surrogate components analyzed by the above system were calibrated by repeated analysis of a standard mixture containing these compounds, and verified by injecting and sampling known amounts of the compound in calibration chamber of known volume. The amounts of gaseous compounds injected were determined by vacuum methods, using an MKS Baratron precision pressure gauge, and bulbs of known volume, determined by weighing when filled with water. The amounts of liquid compounds injected were determined by measuring amounts injected using microliter syringes. The volumes of the calibration chambers were determined by injecting and analyzing compounds whose analyses have been calibrated previously.

The methyl iodide analyses were calibrated by injecting a quantitative amount of methyl iodide in the chamber reactors. The chamber reactors have a known volume and therefore contain a known concentration of methyl iodide. Conducting a GC analysis, a calibration factor was then determined and was used for the duration of the study.

As indicated in Table 2, aerosol number and size distributions were also measured in conjunction with our experiments. However, a discussion of the aerosol data obtained is beyond the scope of this report. This will be described in a separate publication, which is in preparation (Warren et al, 2007).

Most of the instruments other than the GCs and aerosol instrument were interfaced to a PC-based computer data acquisition system under the control of a LabView program written for this purpose. These data, and the GC data from the HP ChemStation computer, were collected over the CE-CERT computer network and merged into Excel files that are used for applying span, zero, and other corrections, and preparation of the data for modeling.

Sampling methods

Samples for analysis by the continuous monitoring instrument were withdrawn alternately from the two reactors and zero air, under the control of solenoid valves that were in turn controlled by the data acquisition system discussed above. For most experiments the sampling cycle was 5 minutes for each reactor, the zero air, or (for control purpose) the chamber enclosure. The program controlling the sampling sent data to the data acquisition program to indicate which state was being sampled, so the data could be appropriately apportioned when being processed. Data taken less than 3-4 minutes after the sample switched were not used for subsequent data processing. The sampling system employed is described in more detail by Carter (2002).

Samples for GC analysis of surrogate compounds were taken at approximately every 20-minute directly from each of the reactors through the separate sample lines attached to the bottom of the reactors. The GC sample loops were flushed for a desired time with the air from reactors using pump.

Characterization Methods

Use of chamber data for mechanism evaluation requires that the conditions of the experiments be adequately characterized. This includes measurements of temperature, humidity, light and wall effects characterization. Wall effects characterization is discussed in detail by Carter (2004) and updated by Carter and Malkina (2005) and Carter (2007) and most of that discussion is applicable to the experiments for this project. The instrumentation used for the other characterization measurements is summarized in Table 2, above, and these measurements are discussed further below.

Temperature was monitored during chamber experiments using calibrated thermocouples attached to thermocouple boards on our computer data acquisition system. The temperature in each of the reactors was continuously measured using relatively fine gauge thermocouples that were located ~1' above the floor of the reactors. These thermocouples were not shielded from the light, though it was hoped that irradiative heating would be minimized because of their small size. Experiments where the thermocouple for one of the reactors was relocated to inside the sample line indicated that radiative heating is probably non-negligible, and that a correction needs to be made for this by subtracting ~2.5°C from the readings of the thermocouples in the reactors. This is discussed by Carter (2004).

Light Spectrum and Intensity. The spectrum of the light source in the 300-850 nm region was measured using a LiCor LI-1800 spectroradiometer, which is periodically calibrated at the factory. Spectroradiometer readings were taken several times during a typical experiment, though the relative spectra were found to have very little variation during the course of these experiments. The absolute light intensity is measured by carrying out NO₂ actinometry experiments periodically using the quartz tube method of Zafonte et al (1977) modified as discussed by Carter et al (1995a). In most cases the quartz tube was located in front of the reactors. Since this location is closer to the light than the centers of the reactors, the measurement at this location is expected to be biased high, so the primary utility of these data are to assess potential variation of intensity over time. However, several special actinometry experiments were conducted prior to the experiments carried out for this project where the quartz tube

was located inside the reactors, to provide a direct measurement of the NO₂ photolysis rates inside the reactors.

Experimental Procedures

The reaction bags were collapsed to the minimum volume by lowering the top frames, and then emptying and refilling them at least six times after each experiment, and then filling them with dry purified air on the nights before experiments. Span measurements were generally made on the continuous instruments prior to injecting the reactants for the experiments. The reactants were then injected through Teflon injection lines (that are separate from the sampling lines) leading from the laboratory below to the reactors. The common reactants were injected in both reactors simultaneously, and were mixed by using the reactor-to-reactor exchange blowers and pipes for 10 minutes. The valves to the exchange system were then closed and the other reactants were injected to their respective sides and mixed using the in-reactor mixing blowers and pipes for 1 minute. The contents of the chamber were then monitored for at least 30 minutes prior to irradiation, and samples were taken from each reactor for GC analysis.

Once the initial reactants are injected, stabilized, and sampled, the light or lights employed (argon arc or blacklights) are turned on to begin the irradiation. During the irradiation the contents of the reactors are kept at a constant positive pressure by lowering the top frames as needed, under positive pressure control. The reactor volumes therefore decrease during the course of the experiments, in part due to sample withdrawal and in part due to small leaks in the reactor. A typical irradiation experiment ended after about 6 hours, by which time the reactors are typically down to about half their fully filled volume. Larger leaks are manifested by more rapid decline of reactor volumes, and the run is aborted early if the volume declines to about 1/3 the maximum. This was not the case for the experiments discussed in this report. After the irradiation the reactors were emptied and filled six times as indicated above.

The procedures for injecting the various types of reactants were as follows. The NO, and NO₂ were prepared for injection using a vacuum rack. Known pressures of NO, measured with MKS Baratron capacitance manometers, were expanded into Pyrex bulbs with known volumes, which were then filled with nitrogen (for NO) or purified air (for NO₂). In order to maintain constant NO/NO₂ ratios the same two bulbs of specified volume were utilized in most of experiments. The contents of the bulbs were then flushed into the reactor(s) with nitrogen. Some of the gaseous reactants such as propylene (other than for surrogate experiments) were prepared for injection using a high vacuum rack as well. For experiments with added CO, the CO was purified by passing it through an in-line activated charcoal trap and flushing it into the reactor at a known rate for the amount of time required to obtain the desired concentration. Measured volumes of volatile liquid reactants were injected, using a micro syringe, into a 2 ft long Pyrex injection tube surrounded with heat tape and equipped with one port for the injection of the liquid and other ports to attach bulbs with gas reactants. For injections into both reactors (e.g. the NO_x and base ROG surrogate components in incremental reactivity experiments), one end of the injection tube was attached to the "Y"-shape glass tube (equipped with stopcocks) that was connected to reactors and the other end of injection tube was connected to a nitrogen source. The injections into a single reactor (e.g., for methyl iodide in the reactivity experiments) was similar except the "Y" tube was not used.

The procedures for injection of the hydrocarbon surrogate components were as follows. A cylinder containing n-butane, trans-2-butene, propylene and ethylene in nitrogen, was used for injecting the gaseous components of the surrogate. The cylinder was attached to the injection system and a gas stream was introduced into reactors at controlled flow for certain time to obtain desired concentrations. A prepared mixture with the appropriate ratios of toluene, n-octane and m-xylene was utilized for injection of these surrogate components, using the procedures as discussed above for pure liquid reactants. All the gas and liquid reactants intended to be the same in both reactors were injected at the same time. The injection consisted of opening the stopcocks and flushing the contents of the bulbs and the liquid reactants

with nitrogen, with the liquid reactants being heated slightly using heat that surrounded the injection tube. The flushing continued for approximately 10 minutes.

The methyl iodide was injected, using a microsyringe, into a glass injection tube leading into the reactor to be employed for the compound. The procedure is the same as used for the liquid hydrocarbon surrogate components.

Materials

The sources of the NO, CO and the various base case surrogate compounds came from various commercial vendors as employed in previous projects at our laboratory. The methyl iodide was purchased from Fisher Scientific, with a stated purity of $\geq 99.5\%$. No significant impurities were detected in any of the GC analyses of these samples.

MECHANISM AND MODELING METHODS

Base Mechanism

The starting point for the chemical mechanism evaluated in this work is the SAPRC-07 mechanism as documented by Carter (2007). This is a complete update of the SAPRC-99 mechanism of Carter (2000a), but it is very similar to it in its major features. The reactions and rate constants in this mechanism are given in tables in Appendix A to this report, and a complete listing of this mechanism, and its documentation, are given by Carter (2007). Files and software implementing this chemical mechanism are in preparation and will also be made available at the SAPRC mechanism web site¹, with the chemical mechanism simulation computer programs available there being essentially the same as those employed in this work.

As discussed previously (Carter, 2000a,b, 2007), the current SAPRC mechanisms consists of a “base mechanism” that represents the reactions of the inorganic species and common organic products and lumped organic radical model species and “operators”, and separate mechanisms for the initial reactions of the many types other organic compounds that are not in the base mechanism. The compounds, or groups of compounds, that are not included in the base mechanism but for which mechanism assignments have been made, are referred to as detailed model species. The latter include all the base ROG surrogate constituents and compounds whose reactivities are being assessed (methyl iodide in this case). These compounds can either be represented explicitly, with separate model species with individual reactions or sets of reactions for each, or using lumped model species similar to those employed in the “fixed parameter” version of SAPRC (Carter, 2000b, 2007). The latter approach is used when modeling complex mixtures in ambient simulations or simulations of experiments with complex mixtures, but the other approach, representing each compound explicitly, is more appropriate when evaluating mechanisms for individual compounds or simple mixtures. This is because the purpose of mechanism evaluations against chamber data is to assess the performance of the mechanism itself, not to assess the performance lumping approaches. The latter is most appropriately assessed by comparing simulations of explicit and condensed versions of the same mechanism in ambient simulations.

In this work, all of the organic constituents in the environmental chamber experiments were represented explicitly using separate model species for each compound, while complex mixture of emitted species in the atmospheric reactivity simulations were represented using the appropriate lumped model species for the fixed parameter mechanism, as indicated in Table A-1 in Appendix A. The reactions and rate constants in the base mechanism are given in Table A-2, and the photolysis rates used are given in Table A-3. These photolysis rates were calculated from applicable actinic flux or light source characterization data and absorption cross-sections and quantum yields given by Carter (2007).

As discussed by Carter (2007) the SAPRC-07 mechanism has a tendency to underpredict rates of O₃ formation in some lower NO_x surrogate - NO_x experiments carried out under lower reactive organic gas (ROG) / NO_x ratios, and this was observed in the model simulations of one of the base case experiments carried out for this project. This is attributed to possible problems in the mechanisms used for the aromatics, which are uncertain. In order to investigate whether this caused biases in predictions of incremental effects of methyl iodide addition on these experiments, test calculations were conducted with the formation of photoreactive products in the toluene and m-xylene mechanisms adjusted upwards to remove this bias. This adjustment consisted of doubling the yield of the model species used to represent

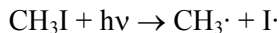
¹ Reports and files concerning the latest version of the SAPRC chemical mechanisms and their associated reactivity scales are available at <http://www.cert.ucr.edu/~carter/SAPRC>.

unsaturated ring fragmentation products that photolyze to form radicals, and setting the yield of those products that photolyze to form stable compounds to zero. This is referred to as the "adjusted aromatics" mechanism in the discussion of the results.

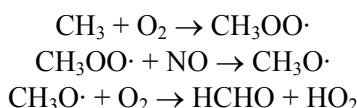
Methyl Iodide Mechanism and Reactions of Iodine Species

The reactions of methyl iodide and the iodine species formed when it reacts were represented explicitly in both the environmental chamber and atmospheric reactivity simulations, and are given on Table 3. Footnotes to Table 3 document the sources of the rate constants and mechanisms used, and this is also discussed below. The absorption cross-sections used for the photolysis reactions are given in Table 4. As indicated in footnotes to Table 3, these reactions are assumed to have unit quantum yields.

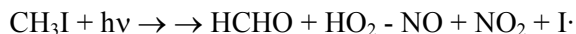
As indicated on Table 3, the major atmospheric loss process for methyl iodide are expected to be photolysis and reactions with OH radicals. The more important of these is photolysis, for which an atmospheric half-life of approximately 1-2 days is calculated based on its absorption cross sections (IUPAC, 2007) and solar actinic flux data (e.g., Peterson, 1976). The reactions is expected to form methyl radicals and Iodine atoms,



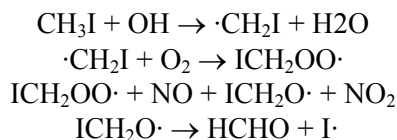
The subsequent reactions of the iodine atoms formed are discussed below. The methyl radicals are expected to react primarily with O₂ and then NO to form formaldehyde and HO₂,



making the overall process



Although photolysis is the major loss process, reaction with OH radicals also occurs to some extent. The expected mechanism is as follows:



This leads to the following overall process:



Note that both the photolysis and reaction with OH radicals are expected to result in the formation of iodine atoms and formaldehyde following an NO to NO₂ conversion. NO to NO₂ conversions are the process responsible for the formation of O₃ in photochemical smog systems, and formaldehyde is also reactive towards ozone formation, so if no other factors were applicable these reactions would indicate that methyl iodide would promote ozone formation. The photolysis reaction also results in the formation of HO₂ radicals, making it a radical initiating process. This means that it would enhance O₃ formation resulting from the reactions of radicals with other VOCs that may be present. However, as discussed below the subsequent reactions of the iodine atoms are not expected to result in the formation of radicals that react with VOCs, so its formation is not a radical initiating or propagating process. This means that the overall effect of the reaction of methyl iodide with OH is radical terminating, which would have a negative effect on O₃ formation from the reactions of radicals with the other VOCs present. However, since photolysis is the relatively more important reaction, the net effect of methyl

Table 3. Mechanism for methyl iodide used in this work.

Label	Reaction and Products [a]	Rate Parameters [b]			Refs & Notes [c]
		k(298)	A	Ea	
Ix01	CH3I + HV = MEO2 + I		Phot Set= CH3I		1,2
Ix02	CH3I + OH = RO2C + xHO2 + xHCHO + I	1.03e-13	4.30e-12	2.23	1,3
Ix03	I + O3 = IO + O2	1.32e-12	2.10e-11	1.65	1
Ix04	I + HO2 = HI + O2	3.96e-13	1.50e-11	2.17	1
Ix05	I + NO2 = INO2	5.05e-12	Falloff, F=0.60, N=1.03 0: 3.00e-31 0.00 -1.00 inf: 6.60e-11 0.00 0.00		1
Ix06	INO2 + HV = I + NO2		Phot Set= BRNO2, Fac= 15.		4
Ix07	IO + HO2 = HOI + O2	8.47e-11	1.40e-11	-1.07	1
Ix08	IO + NO = I + NO2	1.94e-11	7.15e-12	-0.60	1
Ix09	IO + IO = #.15 I2O2 + #.85 {I + I + O2}	9.84e-11	5.40e-11	-0.36	5
Ix10	IO + I2O2 = I3O3	5.00e-12			6
Ix11	IO + I3O3 = I4O4	5.00e-12			6
Ix12	HI + HV = HO2 + I		Phot Set= HI		1
Ix13	HOI + HV = OH + I		Phot Set= HOI		1

[a] Format of reaction listing: “=” separates reactants from products; “#number” indicates stoichiometric coefficient, “#coefficient {product list}” means that the stoichiometric coefficient is applied to all the products listed.

[b] Except as indicated, the rate constants are given by $k(T) = A \cdot (T/300)^B \cdot e^{-E_a/RT}$, where the units of k and A are $\text{cm}^3 \text{molec}^{-1} \text{s}^{-1}$, E_a are kcal mol^{-1} , T is $^{\circ}\text{K}$, and $R=0.0019872 \text{ kcal mol}^{-1} \text{ deg}^{-1}$. The following special rate constant expressions are used:

Phot Set = name: The absorption cross sections for the photolysis reaction are given in Table 4, where “name” indicates the photolysis set used. Unit quantum yields are assumed unless a “Fac=number” notation is given, in which case the number given is the overall quantum yield or adjustment factor, which is assumed to be wavelength independent.

Falloff: The rate constant as a function of temperature and pressure is calculated using $k(T,M) = \{k_0(T) \cdot [M] / [1 + k_0(T) \cdot [M] / k_{inf}(T)]\} \cdot F^Z$, where $Z = \{1 + [\log_{10} \{k_0(T) \cdot [M] / k_{inf}(T)\} / N]^2\}^{-1}$, [M] is the total pressure in molecules cm^{-3} , F and N are as indicated on the table, and the temperature dependences of k_0 and k_{inf} are as indicated on the table.

[c] Footnotes documenting sources of rate constants and mechanisms are as follows.

- 1 Rate constant or absorption coefficients based on IUPAC (2006) recommendation. Unit quantum yields are assumed for photolysis reactions. Mechanism is also as recommended by IUPAC (2006).
- 2 MEO2 is methyl peroxy radicals, whose reactions are given in Table A-2 in Appendix A. Its major fate is reaction with NO to form formaldehyde and HO₂.
- 3 See text for the individual reactions represented by this overall process, and see Table A-1 for a description of the model species used. As indicated there, "RO2C" is used to represent the effects of NO to NO₂ conversions in peroxy radical reactions, and xHCHO and xHO₂ represents the formation of formaldehyde and HO₂ radicals, respectively, in reactions of peroxy radicals with NO.

Table 3 (continued)

- 4 No information is available concerning this reaction, but based on data for ClNO₂ and BrNO₂, the photolysis of INO₂ is expected to be fast. Based on the fact that the absorption cross-sections for BrNO₂ are higher than those for ClNO₂ (IUPAC, 2006), it is expected that INO₂ will photolyze more rapidly than BrNO₂. The absorption cross sections of BrNO₂ are used, but scaled up by a factor of 15, which is derived, in conjunction with adjusting the product yield parameters for Reaction Ix09, to give the best fits to the chamber data obtained in this work. This is represented as a "quantum yield" in the mechanism implementation software, but it is actually an overall photolysis rate adjustment factor. It is expected that the reaction would have a quantum yield of 1.
- 5 The total rate constant is the IUPAC (2006) recommendation. Four overall pathways are considered:



The IUPAC (2006) recommendation is that pathway (1) occurs less than 5% of the time and that pathway (3) occurs ~38% of the time under atmospheric conditions. No recommendations are given concerning the remaining pathways. However, the subsequent reactions of OIO are uncertain and no recommendations are given. In this work, we represent all the possible pathways as either the formation of I atoms (pathway 2) or I₂O₂ (pathway 4), and that the net effect of pathway (3), if it occurs, can be represented by a combination of pathways (2) and (4). Note that major fate of I₂O₂ is assumed to be the formation of unreactive condensed material, i.e., removal of reactive iodine from the system, while the formation of I atoms results in subsequent reactions destroying O₃. The branching ratios for these reactions are adjusted, in conjunction with adjustment of the overall photolysis rate of INO₂ and the rate constants used for reactions of IO with IO oligomers, to give the best fits of the model calculations to the chamber data.

- 6 In order to account for the observed formation of PM in these methyl iodide experiments (Warren et al, 2007) and in previous experiments with diiodomethane (Jimenez et al, 2003), and also to account for the iodine sink needed in the mechanism for the model to predict the effects of methyl iodide reactions on O₃, we assume that formation of condensable IO oligomers occurs from the reactions of IO with IO and the reactions of IO with I_xO_x oligomers. The rate constant is unknown and is a guess. It is expected to be reasonably rapid but not as rapid as the radical + radical and radical + NO_x reactions of these species. Since generally satisfactory simulations were obtained after adjustments to the other uncertain parameters discussed above, it was not necessary to adjust this rate constant as well. It is assumed that I₄O₄ and higher oligomers exist primarily in the condensed phase and do not undergo gas-phase reactions. The modeling of PM formation is beyond the scope of this work, and will be discussed in a separate publication (Warren et al, 2007).

Table 4. Absorption cross-sections used for the photolysis reactions in the methyl iodide mechanism.

Absorption cross section data [a]									
Phot Set = CH3I		Phot Set = BRNO2		Phot Set = HI		Phot Set = HOI			
Wl	Abs	Wl	Abs	Wl	Abs	Wl	Abs	Wl	Abs
280	2.80e-19	280	8.80e-19	280	8.94e-20	280	7.70e-21	460	2.42e-19
285	1.52e-19	285	6.30e-19	285	6.37e-20	285	2.26e-20	465	1.50e-19
290	7.79e-20	290	4.40e-19	290	4.51e-20	290	5.89e-20	470	9.04e-20
295	3.92e-20	295	3.00e-19	295	3.17e-20	295	1.37e-19	475	5.25e-20
300	2.03e-20	300	2.00e-19	300	2.23e-20	300	2.86e-19	480	2.96e-20
305	1.09e-20	305	1.50e-19	305	1.52e-20	305	5.41e-19	485	1.61e-20
310	6.19e-21	310	1.10e-19	310	1.01e-20	310	9.26e-19	490	8.60e-21
315	3.56e-21	315	1.10e-19	315	6.53e-21	315	1.45e-18	496	0
320	2.15e-21	320	1.00e-19	320	4.09e-21	320	2.07e-18		
325	1.24e-21	325	1.20e-19	325	2.47e-21	325	2.72e-18		
330	7.00e-22	330	1.30e-19	330	1.45e-21	330	3.29e-18		
335	3.30e-22	335	1.40e-19	335	8.30e-22	335	3.70e-18		
340	2.30e-22	340	1.60e-19	340	4.70e-22	340	3.85e-18		
345	1.27e-22	345	1.50e-19	347	0	345	3.77e-18		
350	6.70e-23	350	1.60e-19			350	3.47e-18		
355	2.60e-23	355	1.60e-19			355	3.04e-18		
360	1.30e-23	360	1.80e-19			360	2.58e-18		
365	4.00e-24	365	1.90e-19			365	2.21e-18		
370	0	370	1.70e-19			370	1.98e-18		
		375	1.80e-19			375	1.94e-18		
		380	1.70e-19			380	2.07e-18		
		385	1.70e-19			385	2.33e-18		
		390	1.60e-19			390	2.66e-18		
		395	1.50e-19			395	2.98e-18		
		400	1.40e-19			400	3.22e-18		
		405	1.40e-19			405	3.32e-18		
		410	1.30e-19			410	3.27e-18		
		415	1.20e-19			415	3.07e-18		
		420	1.10e-19			420	2.75e-18		
		425	1.00e-19			425	2.35e-18		
		430	9.00e-20			430	1.92e-18		
		435	8.00e-20			435	1.50e-18		
		440	7.00e-20			440	1.13e-18		
		445	7.00e-20			445	8.13e-19		
		450	6.00e-20			450	5.63e-19		
		480	0			455	3.76e-19		

[a] Wavelengths are in nm and absorption cross-sections in cm^2 . The IUPAC (2006) recommendation used for absorption cross sections. Unit quantum yield assumed except as indicated on Table 3.

iodide's reactions is radical initiating, which means it should have a positive effect on O₃ formation if no other factors were important.

The major uncertainties in the methyl iodide mechanism concern the reactions and subsequent fate of the iodine atoms formed in both the photolysis and the OH reaction. Fortunately, a number of the reactions of iodine atoms and the IO_x species it is expected to form have been studied, and available data and recommendations concerning the rate constants and mechanisms are given in the most recent IUPAC (2006) recommendations. However, the available data are not sufficient to unambiguously determine all aspects of the mechanism that may be important in affecting O₃ formation. This is discussed below.

Depending on the experiment, the major loss process for iodine atoms is reaction with O₃ forming IO radicals, or reaction with NO₂ forming INO₂. The former reaction causes direct destruction of O₃ and if it occurs to a sufficient extent it would cancel out the positive effects of the other aspects of the mechanism on O₃ formation and make methyl iodide a net O₃ inhibitor. The formation of INO₂ is only a temporary iodine sink, since it is expected to photolyze rapidly to form re-form iodine atoms and NO₂. However, the existence of this temporary sink is important because the mechanism cannot adequately simulate the results of the chamber experiments if the photolysis is assumed to be so rapid that the formation of INO₂ can be ignored. The reaction of I with HO₂ is relatively unimportant under conditions where O₃ formation occurs, but it may be non-negligible if NO_x is absent and O₃ is sufficiently low.

Most of the uncertainties in the mechanism concern the reactions of the IO formed when I atoms react with O₃. In terms of reaction rate under conditions where O₃ formation occurs, the major process is reaction of IO with NO, forming NO₂ and re-generating iodine atoms. This recycling of iodine atoms permits one iodine atom to react with many molecules of O₃, with the amount of O₃ destruction being determined by the relative importances of the reactions that remove reactive iodine from the system, which occur at much lower rates. However, this I + O₃ → IO; IO + NO → I + NO₂ cycle also involves NO to NO₂ conversions, which tend to promote O₃ formation in these NO_x-air photooxidation systems. Therefore, the amount of O₃ destroyed in this cycle is much less than the number of times it occurs.

The reactions that ultimately determine how much of this iodine cycling occurs are the net iodine sink reactions. The formation of INO₂ is one sink, and although it is a temporary, its importance, as determined by the INO₂ photolysis rate, has an effect on the model simulations of the chamber experiments. This photolysis rate is uncertain and had to be derived based on adjustments to fit the chamber data, but this adjustment is uncertain because adjustments also had to be made for other uncertain iodine sink reactions, as discussed below. The reactions of I and IO with HO₂, forming HI and HOI, respectively, are also temporary sinks, but these are relatively unimportant under conditions where O₃ formation occur, and their rates (both formation and photolysis back to reactive iodine) are also less uncertain.

The results of these methyl iodide experiments cannot be successfully simulated by model calculations unless it is assumed that there are other, more permanent, sinks for reactive iodine species formed in this system. This is despite the fact that most known gas-phase iodine species that might be formed in this system are sufficiently photoreactive that they cannot be sufficient sinks. However, Jimenez et al (2003) observed significant particle formation in the photooxidation of diiodomethane (CH₂I₂), which is expected to react to form similar species as methyl iodide, though much more rapidly because of its higher photolysis rate. Significant particle formation is also observed in the methyl iodide experiments for this project, though a discussion of this is beyond the scope of this report (Warren et al, 2007). This suggests that the major reactive iodine sink is formation of low-volatility oligomeric or polymeric species.

The most likely low-volatility products are oligomers of IO, such as I₂O₂, I₃O₃, etc. I₂O₂ is one of the several possible products of the IO + IO reaction, though as discussed in Footnote 5 to Table 3 the products formed in that reaction are somewhat uncertain. Although the reactions of IO with I₂O₂ or higher oligomers have not been studied, it is not unreasonable to expect that they may occur, and can explain the observed formation of condensable products (Jimenez et al, 2003, Warren et al, 2007). A possible reactive iodine sink mechanism that could account for their formation shown on Table 3. The yields I₂O₂ in the IO + IO reaction, and the rate constants for the IO + I₂O₂ and IO + I₃O₃ reactions are uncertain, and were adjusted to optimize fits of model calculations to the results of the environmental chamber experiments. The photolysis rate for INO₂ was also adjusted as part of this optimization, and because of possible compensating errors these adjustments must be considered to be uncertain. However, using higher or lower INO₂ photolysis rates than shown on Table 3 and optimizing the other parameters did not give as satisfactory results as the combination of parameters shown on the table. Because of this, the mechanism on Table 3 represents our current "best estimate" mechanism for the atmospheric reactions of methyl iodide and the iodine species that it forms.

The ability of this mechanism to simulate the ozone reactivity data in the experiments for this project is given in the Results section of this report, below. This mechanism was also found to give reasonably satisfactory simulations of the particle formation observed in these chamber experiments, as will be discussed in a separate report that is in preparation (Warren et al, 2007).

Representation of Chamber Conditions

The procedures used in the model simulations of the environmental chamber experiments for this project are based on those discussed in detail by Carter (2004) and employed in the studies of Carter and Malkina (2005) and Carter et al (2005b), updated for SAPRC-07 as discussed by Carter (2007). Carter (2004) should be consulted for details of the characterization model and chamber effects parameters employed. The temperatures used when modeling were the averages of the temperatures measured in the reactors, corrected as discussed by Carter (2004). The light intensity for the blacklight experiments varied with time, and the NO₂ photolysis rate for those experiments was derived as discussed in the "Characterization Results" section, below. The blacklight spectral distribution given by Carter et al (1995a) was found to be appropriate for the blacklights in this chamber and was therefore used when modeling the runs discussed in this report.

The chamber effects parameters used when modeling the experiments in this chamber were the same as those given by Carter (2004) except for the HONO offgasing parameters, which were derived based on results of characterization runs carried out in conjunction with these experiments. As discussed by Carter (2004), the chamber effects model currently used for this chamber represents both the chamber radical source and background NO_x offgasing by HONO offgasing, whose magnitude is determined by the chamber effects parameter RN-I, which is the ratio of the HONO offgasing rate to the NO₂ photolysis rate. The RN-I parameter that best fits the characterization data tends to vary over time depending on the conditions of the chamber, and the results of the characterization experiments applicable to modeling the experiments discussed in this report, and the assignment of the RN-I values used, are given in the Characterization Results section, below.

The initial reactant concentrations used in the model simulations were based on the experimentally measured values. However, the calibration of the methyl iodide measurements were based on calculated amounts of methyl iodide injected and the volume of the reactors, which were measured by injecting known quantities of CO or NO_x, and measuring the CO or NO_x using instruments that were independently calibrated.

Atmospheric Reactivity Simulations

Atmospheric reactivity model simulations were carried out to derive MIR and other atmospheric reactivity values for methyl iodide. The base mechanism, scenarios, and methods used were the same as those used when calculating the MIR and other atmospheric ozone reactivity scales for the SAPRC-07 mechanism by Carter (2007), so the atmospheric reactivities calculated for methyl iodide reactivities in this work are directly comparable with those given by Carter (2007) for the ~1100 other types of VOCs represented using the SAPRC-07 mechanism. The mechanism used for methyl iodide and the iodine species it forms were the same as employed in the chamber simulations, as given in Table 3, above, and the mechanisms and rate constants for the reactions of the other species are given in Table A-2 and Table A-3 in Appendix A. The inputs used in the reactivity scenarios are described by Carter (1994a,b).

In order to more systematically assess how atmospheric reactivities of methyl iodide varied with NO_x conditions, a series of reactivity simulations were carried out using the "Averaged Conditions" scenario with NO_x inputs systematically varied. The inputs of those scenarios, other than the total NO_x emissions that were varied, were derived by averaging the conditions of the base case reactivity assessment scenarios. These inputs are also given by Carter et al (1994a,b).

RESULTS AND DISCUSSION

A chronological listing of the environmental chamber experiments carried out for this project is given in Table 5. These include experiments with methyl iodide and appropriate characterization and control experiments needed for the data to be useful for mechanism evaluation. The results of the characterization experiments will be discussed first, followed by a discussion of the results of the mechanism evaluation experiments and of the model simulations of these experiments.

Characterization Results

The results of the individual characterization experiments that are relevant to the experiments for this project are summarized in the “Results” column of Table 5. These and other characterization results relevant to this project are discussed below.

Light Characterization

All experiments carried out for this project used the blacklight light source. Methods for characterizing the intensity of this light source were discussed by Carter et al (2005a), though some revisions were made as a result of subsequent measurements, as discussed by Carter and Malkina (2007). As with the arc light source, NO₂ actinometry measurements were made using the quartz tube method of Zafonte et al (1977), modified as discussed by Carter et al (1995a), with the quartz tube both inside the reactors and also in front of the reactors. As discussed by Carter et al (2005b), the results of these measurements, and other measures of light intensity, indicated a steady decline in light intensity with time, with the results being best correlated with the “blacklight run count”, which is the number of experiments carried out in the chamber using the blacklights, and is thus an indicator of the ageing of the lights due to use. A plot of the results of the in- and out-of-reactor actinometry measurements against run count is shown on Figure 3.

The actinometry measurements made in front of the reactor as shown on Figure 3 are corrected by a factor of 0.698 to give an estimate of the corresponding light intensity inside the reactor. As discussed by Carter et al (2005b), this was derived from near-simultaneous actinometry measurements made both inside and in front of the reactor. Both measurements show similar declines in intensity with time, though the measurements in front of the reactor are more comprehensive because of the larger number of measurements and the larger period of time for which measurements were made.

The actinometry measurements using the blacklight lights source are reasonably well fit by the following empirical expression, where k_1 is the NO₂ photolysis rate in min⁻¹:

$$k_1 = 0.0953 \times [1 + \exp(-\text{Blacklight Run Count} \times 0.00355)] \quad (\text{I})$$

The parameters in Equation (I) were derived to minimize sum-of-squares errors in predictions of both the in-reactor actinometry measurements and the in-front-of-reactor measurements corrected by a factor of 0.698. This equation was used to derive the NO₂ photolysis rates used when modeling the blacklight experiments modeled for this project. Figure 3 indicates the range of blacklight run counts that is applicable to the experiments for this project.

The spectrum of the blacklights in this chamber is measured periodically and continues to be essentially the same as the spectrum recommended by Carter et al (1995a) for modeling blacklight chamber runs.

Table 5. Summary of experiments carried out for this project.

Run [a]	Date	Type [b]	Purpose and Applicable Conditions	Results
718	4/6/07	Surg-MOIR/2 (Side eq)	Side equivalency test. See Table 7	Good side equivalency obtained. See Table 7.
719	4/7/07	CO - Air	Determine background NO _x offgasing. ~60 ppb CO injected.	Similar results obtained for both reactors. Approximately 7 ppb O ₃ formed in ~6 hours. Data simulated using NO _x offgasing rate approximately twice the default for this chamber, which appears to be anomalously high compared to other runs during this period (see Figure 4). The reason for this is not known.
723	4/11/07	Propene - NO _x	Control experiment. ~0.2 ppm propene and ~25 ppb NO _x injected into both reactors.	Similar results obtained for both reactors. ~0.145 ppm O ₃ formed. Results in good agreement with model predictions.
729	4/17/07	CO - NO _x	Determine background radical source. 24 ppb NO _x and 40 ppm CO injected into both reactors.	Results could only be simulated by model if ~0.2 ppb HONO assumed to be present initially, is not normally the case. Results consistent with HONO offgasing parameter in the normal range for runs during this period (see Figure 4).
730	4/18/07	Pure air	Determine background PM formation	~5 ppb of O ₃ formed in approximately 6 hours, which is on the high end of the normal range. The PM results will be discussed in a separate report.
732	4/20/07	Surg-MIR (Side eq)	Side equivalency test. See Table 7	Fair side equivalency obtained. See Table 7.
734	4/23/07	CH ₃ I-NO _x + CO (Side eq)	Mechanism evaluation experiment. See Table 6.	See Table 6 and Figure 6. Same results obtained on both sides.
735	4/24/07	Surg-MIR + CH ₃ I (B)	Mechanism evaluation experiment. See Table 7.	See Table 7 and Figure 8.
736	4/25/07	Surg-MOIR/2 + CH ₃ I (B)	Mechanism evaluation experiment. See Table 7.	See Table 7 and Figure 8.
737	4/26/07	Surg-MOIR/2 + CH ₃ I (A)	Mechanism evaluation experiment. See Table 7.	See Table 7 and Figure 8.
738	4/27/07	CH ₃ I-NO _x + CO (B)	Mechanism evaluation experiment. See Table 6.	See Table 6, Figure 5, and Figure 6.
739	4/28/07	Pure Air	Determine background PM formation	Essentially no measurable O ₃ formed in ~5 hours of irradiation, which is lower than normal. The PM results will be discussed in a separate report

Table 5 (continued)

Run [a]	Date	Type [b]	Purpose and Applicable Conditions	Results
740	4/29/07	Pure Air	Determine background PM formation	Essentially no measurable O ₃ formed in ~5 hours of irradiation, which is lower than normal. The PM results will be discussed in a separate report
741	4/30/07	CO - NO _x	Determine background radical source after methyl iodide experiments conducted. ~60 ppm CO and ~25 ppb NO _x injected into both reactors.	Similar results obtained in both reactors. Change in O ₃ - NO is ~40-50 ppb after 6 hours irradiation. Results in normal range for runs during this period (see Figure 4).
742	5/1/07	O ₃ -CO + CH ₃ I (A)	Mechanism evaluation experiment. See Table 6.	See Table 6, and Figure 7.
743	5/2/07	CH ₃ I - NO _x + CO (B)	Mechanism evaluation experiment. See Table 6.	See Table 6, Figure 5, and Figure 6.
744-747	5/2/07 - 5/5/07	Pure Air	Determine background PM formation after exposure to methyl iodide	The PM results will be discussed in a separate report
748	5/7/07	Surg-MOIR/2 (Side eq)	Side equivalency test. See Table 7	Good side equivalency obtained. See Table 7.

[a] Gaps in run number indicate experiments carried out for other projects.

[b] All experiments are ~6-hour irradiations using blacklights. "Surg" indicates a ROG surrogate - NO_x mixture irradiated; "Surg-MIR" and "Surg-MOIR/2" mean the target initial NO_x and base ROG surrogate were 30 ppb and 0.55 ppmC and 25 ppb and 1.1 ppmC, respectively. "+ reactant (side)" indicates that a reactant was added to the indicated side. "Pure Air" means that no injections were made.

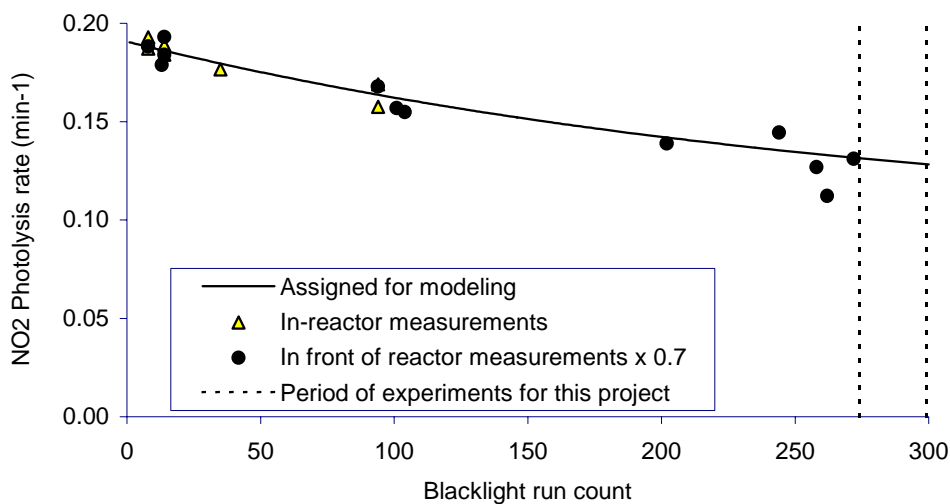


Figure 3. Plots of light intensity data used to assign NO₂ photolysis rates for the blacklight light source.

Chamber Effects Characterization

Except as discussed below, the characterization results for the more recent experiments for this project are consistent with those discussed by Carter et al (2005b) and Carter and Malkina (2005, 2007), and the same characterization parameters were used for modeling. The most important chamber effect, and the only chamber effect parameter that was changed when modeling the experiments for this project, concerns the apparent HONO offgasing, which is believed to be responsible for both the chamber radical source and NO_x offgasing effects (Carter, 2004). This is represented in the chamber effects model by the parameter RN-I, which is the HONO offgasing rate used in the simulations divided by the light intensity as measured by the NO_2 photolysis rate. Figure 4 shows the HONO offgasing parameters that best fit the radical or NO_x - sensitive characterization experiments carried out in the UCR EPA during the period of the last two sets of reactors. Note that the best-fit parameters depend on the mechanism used (particularly the $\text{OH} + \text{NO}_2$ rate constant), and all these were recalculated for SAPRC-07, the mechanism used in this work.

The experiments carried out for this project start at run EPA718, so the applicable characterization data is for the last set of reactors shown on the figure. If the anomalously high RN-I value that fit the data for the data for the CO - air experiment EPA719 is excluded, the average RN-I that fit the data for the runs using these reactors was 8 ppt. This was used when modeling the experiments carried out for this project. For modeling purposes, we use the same chamber effects parameters as used by Carter (2004), Carter and Malkina (2005), and Carter et al (2005b) for all the other chamber effect parameters.

Other chamber characterization experiments carried out during this period were several side equivalency tests (with the same reactive organic gas surrogate - NO_x mixture simultaneously irradiated in both reactors), a propene - NO_x control experiment and several pure air runs. The results of the side equivalency tests indicated acceptable side equivalency and are given in Table 7, in conjunction with the results of the reactivity experiments with methyl iodide, discussed below. The results of the propene - NO_x control run were well simulated by model predictions, as should be the case for such experiments.

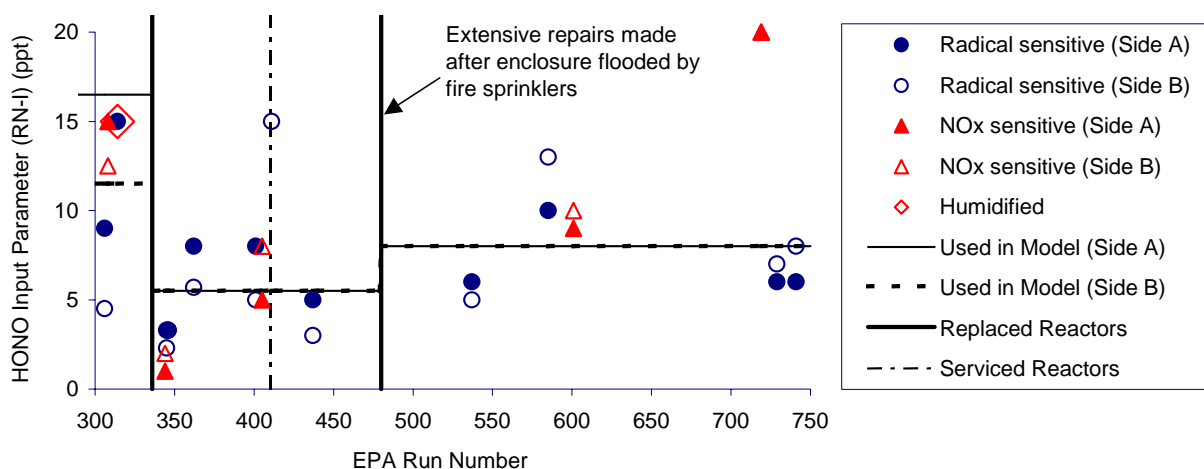
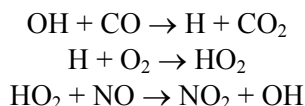


Figure 4. Plots of best fit HONO offgasing parameters against UCR EPA run number.)

The pure air runs were primarily for characterization of background PM formation, and will be discussed in a separate report that is in preparation (Warren et al, 2007). The background O₃ formation was low, which should be the case for this chamber, though the background O₃ in runs 739 and 740 were lower than expected.

Mechanism Evaluation Results

Four types of mechanism evaluation experiments were carried out for this project to test the predictive capability of the methyl iodide mechanism under various types of conditions. Methyl iodide - NO_x and methyl iodide - NO_x + CO experiments were carried out to test the mechanisms for O₃ formation under relatively chemically simple conditions. The methyl iodide - NO_x experiments provided data on NO oxidation and O₃ formation in the absence of other reactions, and the experiments with added CO are useful because the CO reacts with the radicals formed from methyl iodide photolysis to cause NO to NO₂ conversion, and therefore O₃ formation, through its reaction with OH radicals, thus serving as a "radical amplifier".



The O₃ + CO and O₃ + CO + methyl iodide irradiations tested the mechanism for the effects of methyl iodide reactions on O₃ destruction in the absence of NO_x, with the CO being present as a dilution tracer. Finally, incremental reactivity experiments were carried out to provide data to test mechanism predictions of the effects of methyl iodide on O₃ formation in more chemically realistic model photochemical smog systems. These types of experiments are discussed further below.

The initial concentrations and selected results for the first three types of mechanism evaluation experiments are summarized on Table 6, and experimental and calculated concentration-time profiles for the major measured species are shown on Figure 5 through Figure 6. The model simulations shown are the best that could be obtained, and reflect the effects of adjustments of the overall photolysis rate for IONO₂ and the yield of I₂O₂ in the reaction of IO with IO (see Table 3 and footnotes). Simulations of these runs were used as the basis for deriving the values of the parameters used for the best fit mechanism given on Table 3.

Figure 5 shows that in the absence of added CO the O₃ formation in the methyl iodide - NO_x experiments is relatively low, and the main effect of the methyl iodide reactions is the oxidation of NO. The model gives reasonably good simulations of the initial NO oxidation rates in these experiments, though the NO oxidation rate in the latter part of EPA743A is somewhat overpredicted. Methyl iodide is consumed relatively slowly in these experiments, and its consumption rates are reasonably well simulated by the model.

Figure 6 shows that the addition of CO to the methyl iodide - NO_x system causes a significant increase in the initial NO oxidation rates and results in the formation of O₃ if a sufficient amount of CO is added. The NO oxidation rates and initial O₃ formation rates are reasonably well simulated in these experiments, though the model does not simulate the extent to which O₃ formation slows down at the end of the experiments with the higher levels of added CO, and does not simulate the destruction of the low amount of O₃ formed in run 743B at the end of the experiment. The methyl iodide consumption rates are reasonably well simulated except in run 743B, though it should be noted that the consumption rate is relatively slow and small amounts of dilution may affect the model performance in this regard. Although the fits are not perfect, they are probably as good as can reasonably be expected considering the uncertainties in the mechanism, and also characterization uncertainties in the experiments.

Table 6. Summary of initial concentrations and selected results for the methyl iodide - NO_x, methyl iodide - CO - NO_x, and methyl iodide - O₃ - CO irradiations.

Run	Side	Initial concentrations				O ₃ (ppb)		Δ([O ₃]-[NO]) (ppb)	
		CH ₃ I (ppm)	NO _x (ppb)	CO (ppm)	O ₃ (ppb)	2 hr	6 hr	2 hr	6 hr
EPA738	A	0.202	24	-	-	4	9	8	20
EPA743	A	0.500	23	-	-	6	6	13	23
EPA734	A	0.201	24	56	-	53	82	67	98
EPA734	B	0.200	24	57	-	52	82	66	97
EPA738	B	0.201	24	55	-	52	77	66	92
EPA743	B	0.500	23	4	-	16	3	27	20
EPA742	B	-	-	63	102	98	90	-4	-12
EPA742	A	0.344	-	58	95	82	55	-13	-39

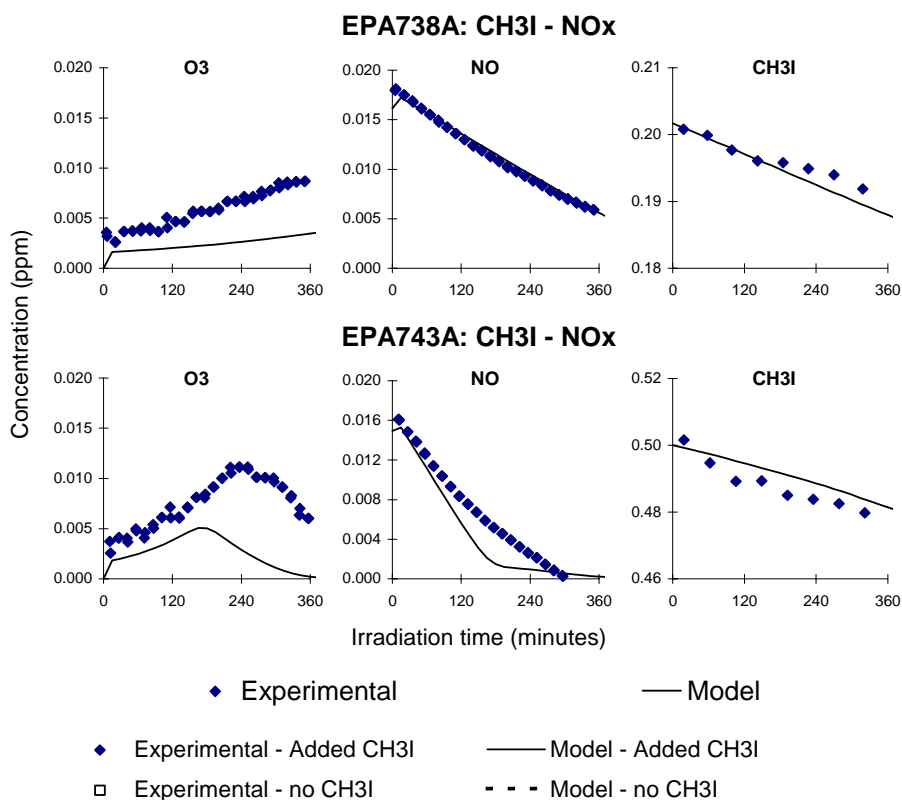


Figure 5. Experimental and calculated results of the methyl iodide - NO_x experiments.

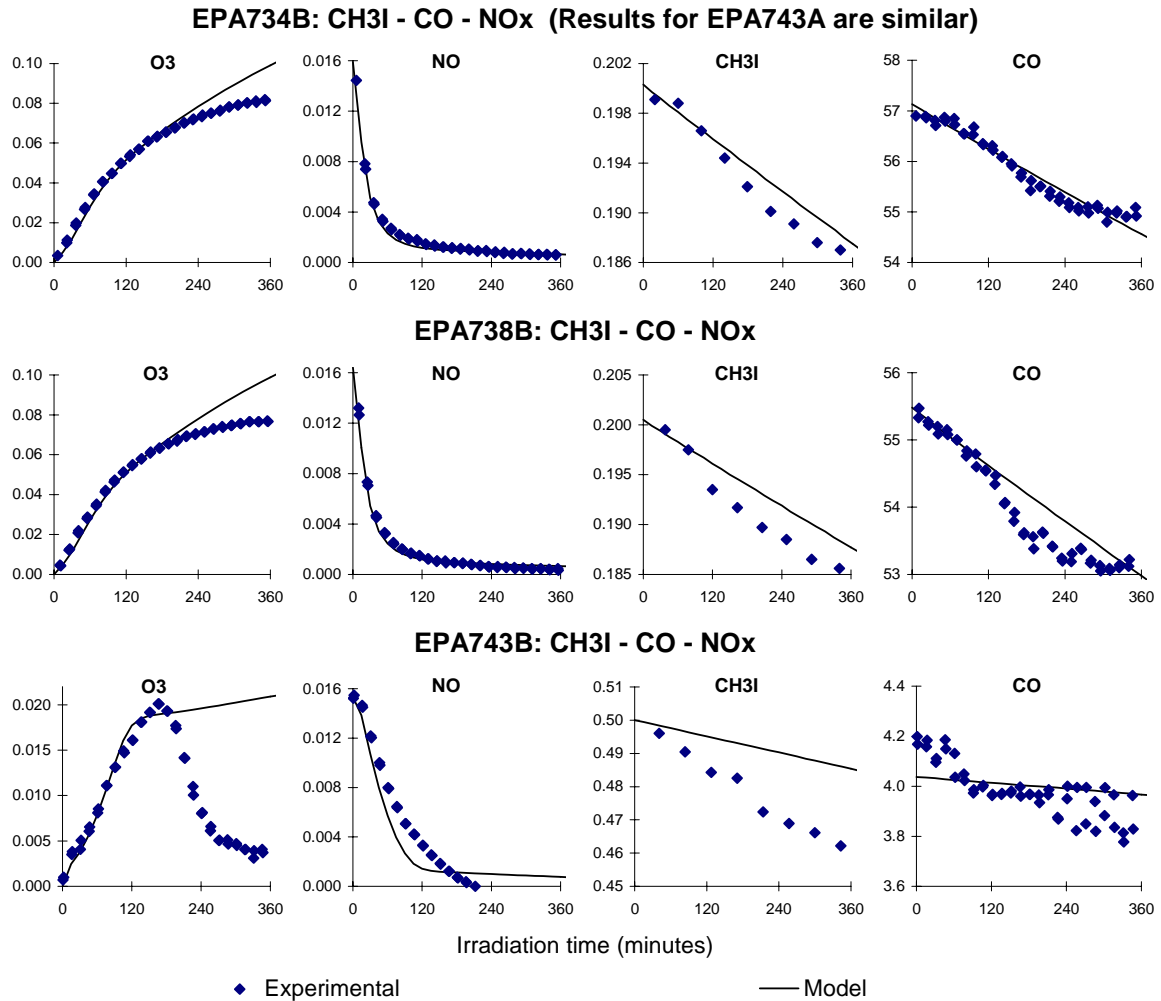


Figure 6. Experimental and calculated results of the methyl iodide + CO - NO_x experiments.

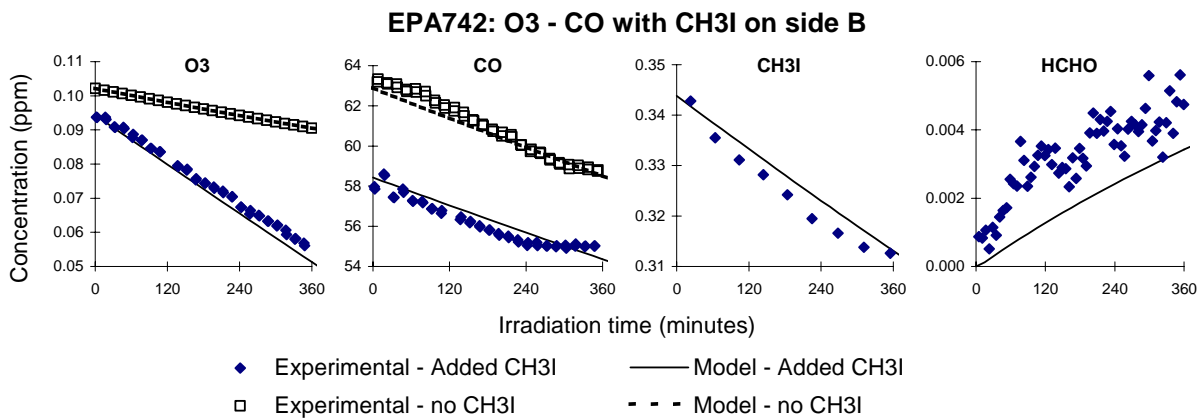


Figure 7. Experimental and calculated results of O₃ - CO and O₃ - CO - Methyl iodide irradiation experiments.

Figure 7 shows that the addition of methyl iodide in the O₃ + CO irradiation system causes an increase in the O₃ consumption rate, though (as expected) the consumption rate of CO is not affected. The model gives a reasonably good simulation of the affect of the methyl iodide. (The consumption of CO is caused primarily by dilution, and the dilution rates in the simulation were adjusted to account for this.) The consumption rate of methyl iodide is reasonably well simulated in this experiment.

Formaldehyde data obtained using the PTRMS was also available during the O₃ + CO + methyl iodide experiment. Figure 7 shows that the measured formaldehyde level was reasonably consistent with model predictions, and indicate that formaldehyde is indeed formed in the methyl iodide photooxidation, as expected. Unfortunately, this instrument was not operational or available during the other experiments employing methyl iodide.

The fact that the same mechanism can give good simulations of the effects of methyl iodide on O₃ consumption in the absence of NO_x and fair to good predictions of its effects on NO oxidation and O₃ formation in the presence of NO_x makes it appear less likely that the model fits are a result of errors in the mechanism that are important in the presence of NO_x (e.g., the INO₂ photolysis rate) compensating for errors in reactions that occur in the absence of NO_x, such as the formation of I₂O₂ from the IO + IO reaction. Note that other sets of values tried for the adjusted rate constants or parameters did not yield simulations that were as good as those shown on Figure 5 through Figure 7.

The conditions and selected results of the incremental reactivity experiments used to evaluate methyl iodides mechanism are summarized on Table 7. Incremental reactivity experiments consist of irradiations of a reactive organic gas (ROG) - NO_x mixture serving as a simplified model of the chemical system involved on O₃ formation in urban atmospheres, together in irradiations of the same mixture with a test compound (methyl iodide in this case) added. The experiment without the added test compound is referred to as the "base case" experiment, and the experiment where the test compound is added is the "test" experiment. The differences in O₃ formation and other measures of reactivity in these experiments provide a measure of the effects of the test compound in a system more closely representing atmospheric conditions than the simpler experiments discussed above, and provide a more realistic test of the mechanism's ability to predict its atmospheric reactivity.

As in previous incremental reactivity experiments carried out in this chamber (Carter and Malkina, 2005, 2007; Carter et al, 2005b), two types of base case experiments are employed. The first is a lower ROG/NO_x experiment designed to approximate conditions where O₃ formation is most sensitive to VOC emissions, which serve as the basis for the MIR reactivity scale, and are referred to as "MIR" experiments. The second is at higher ROG/NO_x ratios with NO_x levels at approximately half that yielding maximum ozone concentrations, and are referred to as "MOIR/2" experiments. In both cases, the base ROG surrogate mixture representing reactive organic gases from all sources consists of n-butane, n-octane, ethene, propene, trans-2-butene, toluene and m-xylene, and is based on a mixture derived previously (Carter et al, 1995b) as a simplification of ambient mixtures used in the atmospheric reactivity calculations. Earlier versions of this mixture also contained formaldehyde, but this was not included in the current experiments for experimental reasons. As discussed by Carter and Malkina (2005), the removal of formaldehyde from the base ROG surrogate mixture does not significantly the utility of the experiments for mechanism evaluation.

The measures of gas-phase reactivity used to evaluate the mechanisms in the incremental reactivity experiments are the effects of the methyl iodide on $\Delta([O_3]-[NO])$, or $([O_3]_t-[NO]_t)-([O_3]_0-[NO]_0)$, and IntOH, the integrated OH radical levels. As discussed elsewhere (e.g., Johnson, 1983; Carter and Atkinson, 1987; Carter and Lurmann, 1991, Carter et al, 1993), $\Delta([O_3]-[NO])$ gives a direct measure of the amount of conversion of NO to NO₂ by peroxy radicals formed in the photooxidation reactions, which is the process that is directly responsible for ozone formation in the atmosphere. This gives a useful

Table 7. Summary of initial concentrations and selected gas-phase results of the incremental reactivity experiments.

Run	Test Side	Type	CH ₃ I Added (ppm)	Base Run Initial Concentrations		Final [a] O ₃ (ppb)		Δ([O ₃]-[NO]) Change (ppb)		IntOH change (ppt-min)
				NO _x (ppb)	ROG (ppmC)	Base	Test	2 Hr	Final [a]	
Side Equivalency Tests										
EPA718	B	MOIR/2		17	1.03	91	90	-3	-3	-2
EPA732	B	MIR		29	0.49	71	76	2	5	-3
EPA748	B	MOIR/2		23	1.12	105	109	1	2	
Methyl Iodide Reactivity										
EPA735	B	MIR	0.201	47	0.47	61	32	27	-27	31
EPA736	B	MOIR/2	0.398	25	1.00	109	33	-14	-75	-2
EPA737	A	MOIR/2	0.213	25	1.09	98	73	-4	-26	1

[a] "Final" is 6-hour value for all runs except for EPA732, for which "final" means 5-hour value.

measure of factors affecting O₃ reactivity even early in the experiments where O₃ formation is suppressed by the unreacted NO. Although this is the primary measure of the effect of the VOC on O₃ formation, the effect on radical levels is also a useful measure for mechanism evaluation, because radical levels affect how rapidly all VOCs present, including the base ROG components, react to form ozone.

The integrated OH radical levels are not measured directly, but can be derived from the amounts of consumption of reactive VOCs that react only with OH radical levels. In particular,

$$\text{IntOH}_t = \frac{\ln([\text{tracer}]_0/[\text{tracer}]_t) - Dt}{k\text{OH}^{\text{tracer}}} \quad (\text{II})$$

where [tracer]₀ and [tracer]_t are the initial and time t concentrations of the compound used as the OH tracer, kOH^{tracer} its OH rate constant, and D is the dilution rate in the experiments. The latter is small in our chamber compared to the tracer consumption rates and is neglected in our IntOH analysis. The base ROG surrogate component m-xylene was used as the tracer to derive the IntOH levels in these experiments. The OH + m-xylene rate constant used was 2.36 x 10⁻¹¹ cm³ molec⁻¹ s⁻¹ (Atkinson et al, 1989).

Plots of experimental Δ([O₃]-[NO]) and IntOH in the base case and test experiments, changes in these quantities caused by adding the methyl iodide, are shown on Figure 8. It can be seen that the addition of the methyl iodide caused an increase in the initial NO oxidation rate in the MIR and (to a much lesser extent) in the MOIR/2 experiments, but it ultimately caused less ozone formation to occur by the end of the experiment, particularly in the MOIR/2 experiments. The methyl iodide had a positive effect on IntOH in the MIR experiment, but relatively little effect on overall radical levels in the lower NO_x MOIR/2 runs. The consumption rate of methyl iodide (not shown) was relatively slow, as was the case in the other experiments shown above.

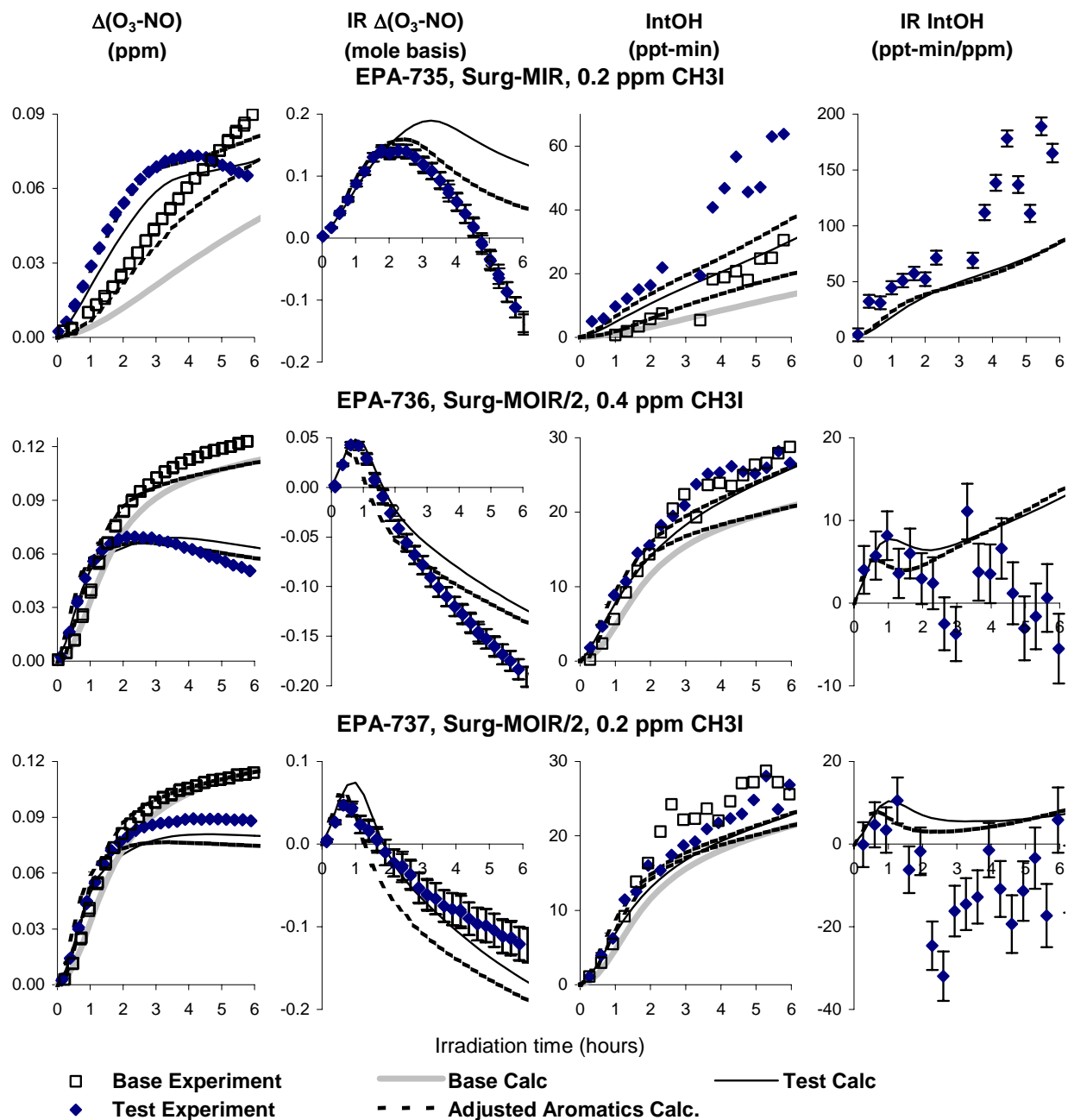


Figure 8. Experimental and calculated results of the incremental reactivity experiments with added methyl iodide.

The results of the model simulations of the reactivity experiments are also shown on Figure 8. Because the standard mechanism tends to underpredict O_3 formation in the base case MIR experiment (see Carter, 2004; Carter et al, 2005a,b and Carter, 2007), model simulations were also carried out with an "adjusted aromatics" mechanism that gave better fits to the base case experiments. It can be seen that the model gives reasonably good predictions of the effect of the methyl iodide on NO oxidation, O_3 formation and integrated OH levels, though there is a tendency to underpredict the rate of O_3 consumption at the end of the MIR experiment and the MOIR/2 experiment with the larger amount of methyl iodide.

Note that the methyl iodide mechanism was not adjusted to optimize fits to the reactivity experiments – all adjustments were based on modeling the simpler experiments discussed above. Since the mechanism can simulate the data reasonably well under a variety of conditions, including those representing atmospheric conditions under different levels of relative NO_x availability, it can be considered to be reasonably well evaluated. It does have a tendency to underpredict the consumption of O₃ at the end of some experiments, suggesting that it may underpredict the extent of O₃ inhibition it may cause under some atmospheric conditions.

Atmospheric Reactivity Calculations

Conditions and maximum O₃ concentrations of the ambient scenarios used for reactivity assessment are summarized on Table 8. These are the same scenarios as used to calculate the atmospheric reactivities of the ~1100 types of VOCs using the SAPRC-07 mechanism by Carter (2007), and are also the same as used in previous reactivity scales calculated using the SAPRC-99 (Carter, 2000a), and SAPRC-90 (Carter, 1994) mechanisms. All of these are 1-day box model scenarios with varying inversion heights, initially present and emitted NO_x and reactive organics, and O₃ and background VOCs entrained from aloft as the inversion heights increase during the day (Carter, 1994a,b), with inputs designed to represent various urban areas around the United States (1990). As discussed previously, four types of scenarios are employed.

- **Base.** The base case scenarios have the NO_x and other inputs as originally specified by Bauges (1990) to represent the various urban areas around the United States. Note that these are not good representations of current conditions, since generally these scenarios predict much higher O₃ levels than currently occur, and these box model incorporate significant simplifications of transport, mixing, and emissions, and multi-day effects, which can be important. However, they do represent a variety of chemical conditions, which are the main factors reflecting *relative* atmospheric reactivities of VOCs. These scenarios represent a variety of relative NO_x levels, which is a major factor affecting absolute and relative reactivities of VOCs (Carter and Atkinson, 1989; Carter, 1994a). For this reason, other types of scenarios, discussed below, are derived to represent standard conditions of NO_x availability.
- **MIR.** The Maximum Incremental Reactivity (MIR) scenarios have the NO_x inputs adjusted so that the base ROG mixture used to represent all the anthropogenic VOC emissions has the maximum incremental reactivity relative to ozone formation. All the other inputs are the same as in the base case scenarios. Although the base ROG reactivity is used to define the MIR NO_x level, most other types of VOCs also have their maximum incremental reactivity at this same NO_x level. These scenarios represent the relatively high NO_x conditions where O₃ formation is the most sensitive to VOC emissions. The averages incremental reactivities in all these scenarios are used to derive the MIR scale that is used in regulatory applications in California (CARB 1993, 2000).
- **MOIR.** The Maximum Ozone Incremental Reactivity (MOIR) scenarios have the NO_x inputs adjusted to give the maximum daily maximum ozone concentration. All other inputs are the same as in the base and MIR scenarios. These scenarios represent NO_x conditions that are optimum for O₃ formation, which is always lower than those for MIR. The averages incremental reactivities in all these scenarios are used to derive the MOIR scale, which can be considered as an alternative to MIR (Carter, 1994a).
- **EBIR.** The Equal Benefit Incremental Reactivity (EBIR) scenarios have the NO_x inputs adjusted so that O₃ formation is equally sensitive to changes in total ROG or NO_x inputs. All the other inputs are the same as in the base, MIR, and MOIR scenarios. The NO_x inputs are always lower than those yielding maximum O₃ (MOIR), and represent the lowest NO_x levels where VOC control is at least as effective as NO_x control. The averages incremental reactivities in all these

Table 8. Summary of conditions of scenarios used for reactivity assessment

Scenario	Max O ₃ (ppb)				ROG / NO _x				Max Height (kM)	ROG input (m.mol m ⁻²)	O ₃ aloft (ppb)	Int'd OH (ppt-min)	Final H (m)
	Base	MIR	MOIR	EBIR	Base	MIR	MOIR	EBIR					
Averaged Conditions		179	227	213		4.0	6.3	9.2	1.8	15	70	118	1823
Atlanta, GA	173	145	177	169	7.3	3.8	5.7	8.1	2.1	12	63	190	2146
Austin, TX	172	154	187	177	9.3	3.6	5.4	8.3	2.1	11	85	174	2108
Baltimore, MD	310	245	321	296	5.2	4.1	6.3	10.2	1.2	17	84	154	1169
Baton Rouge, LA	236	185	236	226	6.8	4.5	6.7	8.9	1.0	11	62	175	968
Birmingham, AL	241	203	260	245	6.9	2.9	4.4	6.5	1.8	13	81	196	1770
Boston, MA	194	165	201	191	6.5	2.9	4.5	6.9	2.6	14	105	236	2598
Charlotte, NC	141	139	164	159	7.8	2.0	3.0	4.2	3.0	7	92	200	3046
Chicago, IL	288	242	322	301	11.6	4.5	6.8	10.1	1.4	25	40	171	1392
Cincinnati, OH	197	158	199	183	6.4	3.5	5.4	9.2	2.8	17	70	196	2816
Cleveland, OH	243	194	243	230	6.6	4.5	7.1	10.5	1.7	16	89	168	1650
Dallas, TX	183	176	204	194	4.7	4.6	6.5	9.3	2.3	18	75	140	2250
Denver, CO	192	161	199	188	6.3	5.1	7.8	11.9	3.4	29	57	129	3358
Detroit, MI	238	184	240	220	6.8	3.9	6.1	10.1	1.8	17	68	210	1844
El Paso, TX	175	145	177	169	6.6	4.7	7.3	10.2	2.0	12	65	129	2000
Hartford, CT	169	149	186	174	8.4	2.9	4.6	7.4	2.3	11	78	204	2318
Houston, TX	300	228	301	280	6.1	4.2	6.3	9.7	1.7	25	65	200	1748
Indianapolis, IN	204	158	204	192	6.6	4.1	6.6	10.0	1.7	12	52	190	1675
Jacksonville, FL	151	126	158	151	7.6	3.7	5.6	7.7	1.5	8	40	195	1485
Kansas City, MO	153	127	159	147	7.1	3.2	5.0	8.6	2.2	9	65	209	2200
Lake Charles, LA	292	231	308	293	7.4	3.7	5.4	7.3	0.5	7	40	224	457
Los Angeles, CA	561	408	563	533	7.6	5.4	8.2	11.5	0.5	23	100	128	503
Louisville, KY	204	163	204	194	5.5	3.3	5.2	7.5	2.5	14	75	231	2518
Memphis, TN	226	179	233	218	6.8	3.4	5.2	7.9	1.8	15	58	227	1750
Miami, FL	130	123	150	144	9.6	2.9	4.5	6.5	2.7	9	57	173	2720
Nashville, TN	163	148	188	177	8.0	2.7	4.0	6.1	1.6	7	50	218	1608
New York, NY	375	302	380	358	8.1	4.9	6.8	10.1	1.5	39	103	152	1512
Philadelphia, PA	235	179	235	220	6.2	4.2	6.4	9.8	1.8	19	53	196	1800
Phoenix, AZ	269	208	269	246	7.6	5.1	7.9	13.1	3.3	40	60	147	3250
Portland, OR	160	133	164	158	6.5	3.2	5.0	7.1	1.6	6	66	211	1575
Richmond, VA	233	180	234	216	6.2	3.7	5.6	9.5	1.9	16	64	191	1932
Sacramento, CA	197	152	198	185	6.6	3.9	6.1	9.3	1.1	7	60	190	1103
St Louis, MO	304	237	313	290	6.1	4.8	7.4	11.9	1.6	26	82	152	1625
Salt Lake City, UT	182	158	191	179	8.5	3.6	5.6	9.2	2.2	11	85	176	2150
San Antonio, TX	120	101	123	119	3.9	3.0	4.8	6.6	2.3	6	60	157	2308
San Diego, CA	185	148	185	177	7.1	4.8	7.4	10.3	0.9	8	90	131	850
San Francisco, CA	211	347	457	436	4.8	6.2	9.3	12.4	0.7	25	70	58	650
Tampa, FL	212	175	220	211	4.4	3.6	5.3	7.2	1.0	8	68	171	991
Tulsa, OK	220	172	220	204	5.3	3.6	5.5	8.9	1.8	15	70	222	1830
Washington, DC	275	214	276	259	5.3	3.3	4.9	7.5	1.4	13	99	210	1421

scenarios are used to derive the EBIR scale, which is a useful complement to the MIR scale in assessing how NO_x levels affect relative reactivities.

- Averaged Conditions. The averaged conditions scenarios have all inputs other than total NO_x derived to represent the average for the base case scenarios. The NO_x inputs are varied to assess how measures of reactivity depend on NO_x with other inputs held constant. Incremental reactivities in the MIR, MOIR, and EBIR averaged conditions scenarios (i.e., whose NO_x inputs are adjusted to represent those respective conditions) usually give good approximations to reactivities in those respective scales, though they are not used in deriving these scales. These scenarios are used in this work to show how the calculated incremental reactivities of methyl iodide depend on NO_x conditions.

Table 9 gives the calculated incremental reactivities for methyl iodide in these various scenarios, and these reactivities are plotted against the input ROG/NO_x ratio in these scenarios in Figure 9. It can be seen that methyl iodide is calculated to have a negative effect on O₃ formation in all the base case scenarios but one, the "San Francisco" scenario². Note that this is the only base case scenario where the NO_x input is lower than that of the corresponding MIR scenario (see Table 8). The incremental reactivities are negative in all the MIR, MOIR, and EBIR scenarios, and they tend to become more negative as the relative NO_x levels decrease. Figure 9 shows that the averaged conditions reactivities are negative in all the averaged conditions scenarios where ROG/NO_x ratios are greater than ~3, but are positive if the ROG/NO_x ratios are lower than that. Since this ratio is lower than that for the averaged conditions MIR scenario (which is ~4), the averaged conditions MIR value is negative.

Figure 9 indicates that the inhibition of O₃ by methyl iodide tends to increase with increasing ROG/NO_x ratio, but that this is not the only factor affecting the impact of this compound. For example, the ROG/NO_x ratio of the base "San Francisco" scenario with the positive methyl iodide reactivity is higher than that of many MIR (and some MOIR and base case) scenarios where the reactivity of methyl iodide is negative. This is because the ROG/NO_x ratio is not the only factor affecting relative NO_x availability; other scenario conditions, such as overall light intensity, absolute concentrations, etc., affect how rapidly NO_x is removed and thus at what point conditions become NO_x-limited. This can be taken into account by using the ratio of the ROG/NO_x ratio to the ROG/NO_x ratio yielding maximum O₃ formation (the MOIR ratio).

A plot of the incremental reactivity of methyl iodide against the ROG/NO_x ratio normalized by the MOIR ROG/NO_x ratio is shown on Figure 10. It can be seen that this gives a much better prediction of how the incremental reactivity of this compound depends on NO_x, and also shows that the reactivity in the base case "San Francisco" scenario is entirely consistent with the trend observed in the other scenarios. It indicates that methyl iodide should have a positive impact on O₃ formation only under NO_x conditions that are approximately twice that yielding maximum O₃ levels, or about 20-25% higher than those yielding maximum incremental reactivity. These represent conditions that are very close to NO_x sources, where O₃ formation is inhibited by NO_x.

Table 9 and Figure 10 also show calculated incremental reactivities for ethane, the compound that has been used by the U.S. EPA as the informal standard to define "negligible" ozone impact for the purpose of exempting VOCs from regulation as ozone precursors (Dimitriades, 1999). It can be seen that although its incremental reactivities are relatively low, they are always positive, with the highest

² Note that this scenario does not necessarily represent the actual current conditions in San Francisco, since the inputs were developed over 17 years ago, and a highly simplified physical model is used. These scenarios, taken as a whole, are mainly useful for representing a range of conditions that can affect reactivity, not necessarily conditions in any particular region.

Table 9. Calculated atmospheric incremental reactivities for methyl iodide and ethane.

Scenario	CH ₃ I Incremental Reactivity (gm O ₃ / gm VOC)				Ethane Incremental Reactivity (gm O ₃ / gm VOC)			
	Base	MIR	MOIR	EBIR	Base	MIR	MOIR	EBIR
<u>Averaged Conditions</u>		-0.54	-2.23	-2.83		0.27	0.18	0.13
<u>Reactivity Scale Value (Scenario averages)</u>	-2.2±0.7	-0.55	-2.11	-2.80	0.17 ±0.04	0.27	0.19	0.13
Atlanta, GA	-2.26	-0.50	-1.83	-2.39	0.14	0.25	0.18	0.13
Austin, TX	-2.51	-0.49	-1.83	-2.43	0.14	0.28	0.21	0.15
Baltimore, MD	-1.65	-0.51	-2.44	-3.42	0.21	0.26	0.18	0.13
Baton Rouge, LA	-2.03	-0.65	-2.00	-2.50	0.13	0.20	0.13	0.09
Birmingham, AL	-3.20	-0.50	-2.32	-3.12	0.18	0.35	0.25	0.19
Boston, MA	-2.50	-0.58	-1.96	-2.56	0.16	0.28	0.20	0.15
Charlotte, NC	-2.70	-0.53	-1.84	-2.32	0.13	0.31	0.25	0.20
Chicago, IL	-3.27	-0.62	-2.36	-3.13	0.09	0.24	0.15	0.10
Cincinnati, OH	-2.29	-0.46	-1.97	-2.74	0.21	0.31	0.23	0.17
Cleveland, OH	-2.04	-0.54	-2.23	-2.95	0.17	0.22	0.16	0.12
Dallas, TX	-0.96	-0.83	-1.84	-2.30	0.24	0.25	0.17	0.12
Denver, CO	-1.22	-0.42	-1.94	-2.78	0.16	0.19	0.12	0.09
Detroit, MI	-2.47	-0.52	-2.23	-2.98	0.19	0.29	0.20	0.15
El Paso, TX	-1.39	-0.38	-1.66	-2.22	0.15	0.19	0.13	0.09
Hartford, CT	-2.83	-0.41	-1.98	-2.73	0.17	0.34	0.25	0.19
Houston, TX	-2.25	-0.66	-2.35	-3.07	0.19	0.28	0.19	0.13
Indianapolis, IN	-2.31	-0.43	-2.30	-2.97	0.19	0.29	0.20	0.14
Jacksonville, FL	-2.38	-0.60	-1.88	-2.39	0.13	0.27	0.17	0.12
Kansas City, MO	-2.39	-0.32	-1.82	-2.56	0.21	0.36	0.26	0.18
Lake Charles, LA	-3.28	-0.85	-2.68	-3.26	0.11	0.30	0.17	0.11
Los Angeles, CA	-2.71	-0.83	-2.99	-3.79	0.09	0.14	0.08	0.06
Louisville, KY	-2.42	-0.63	-2.27	-2.84	0.23	0.34	0.25	0.18
Memphis, TN	-2.86	-0.55	-2.31	-3.05	0.17	0.34	0.21	0.15
Miami, FL	-2.67	-0.49	-1.84	-2.40	0.11	0.30	0.20	0.15
Nashville, TN	-3.01	-0.52	-2.18	-2.83	0.18	0.46	0.31	0.23
New York, NY	-3.07	-0.76	-2.52	-3.55	0.08	0.16	0.09	0.06
Philadelphia, PA	-2.03	-0.53	-2.12	-2.79	0.18	0.27	0.18	0.13
Phoenix, AZ	-1.90	-0.38	-2.03	-2.93	0.20	0.26	0.19	0.13
Portland, OR	-2.36	-0.51	-1.96	-2.46	0.18	0.30	0.22	0.16
Richmond, VA	-2.43	-0.41	-2.18	-3.13	0.19	0.28	0.20	0.15
Sacramento, CA	-2.19	-0.42	-2.02	-2.68	0.20	0.31	0.21	0.15
St Louis, MO	-1.69	-0.55	-2.40	-3.37	0.18	0.21	0.14	0.10
Salt Lake City, UT	-2.51	-0.39	-1.83	-2.60	0.17	0.29	0.22	0.16
San Antonio, TX	-1.06	-0.42	-1.40	-1.73	0.23	0.25	0.19	0.14
San Diego, CA	-1.47	-0.52	-1.54	-1.96	0.10	0.15	0.10	0.07
San Francisco, CA	0.34	-0.82	-2.56	-3.38	0.08	0.11	0.07	0.05
Tampa, FL	-1.58	-0.72	-2.19	-2.70	0.22	0.25	0.16	0.12
Tulsa, OK	-2.22	-0.60	-2.29	-3.05	0.21	0.31	0.21	0.15
Washington, DC	-2.51	-0.61	-2.32	-3.06	0.19	0.29	0.20	0.15

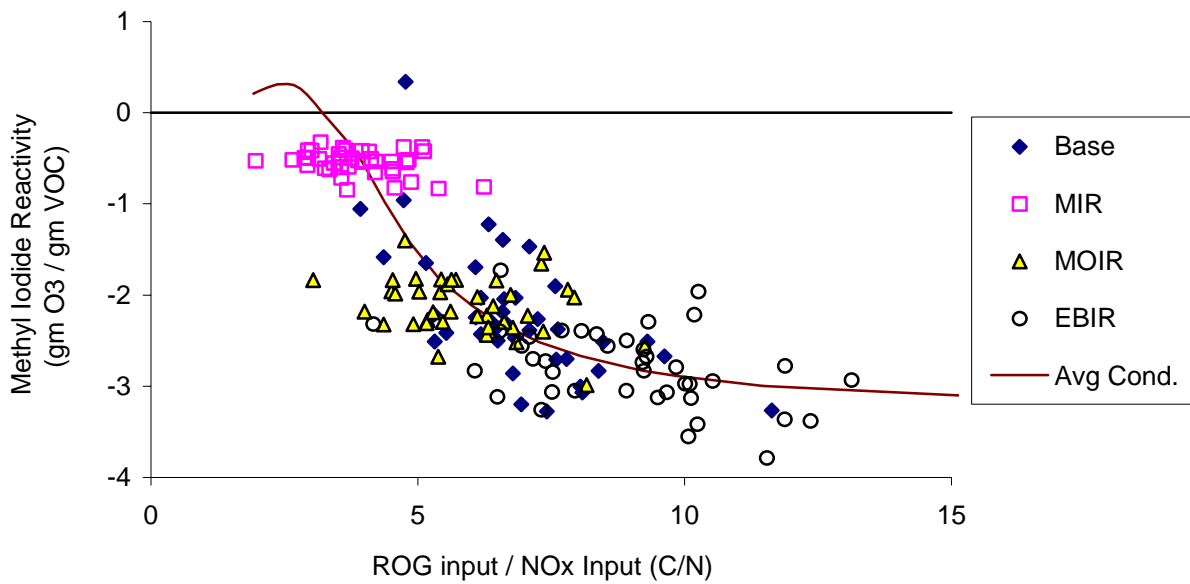


Figure 9. Plots of incremental reactivities of methyl iodide in the atmospheric reactivity scenarios against the ROG / NO_x input ratio.

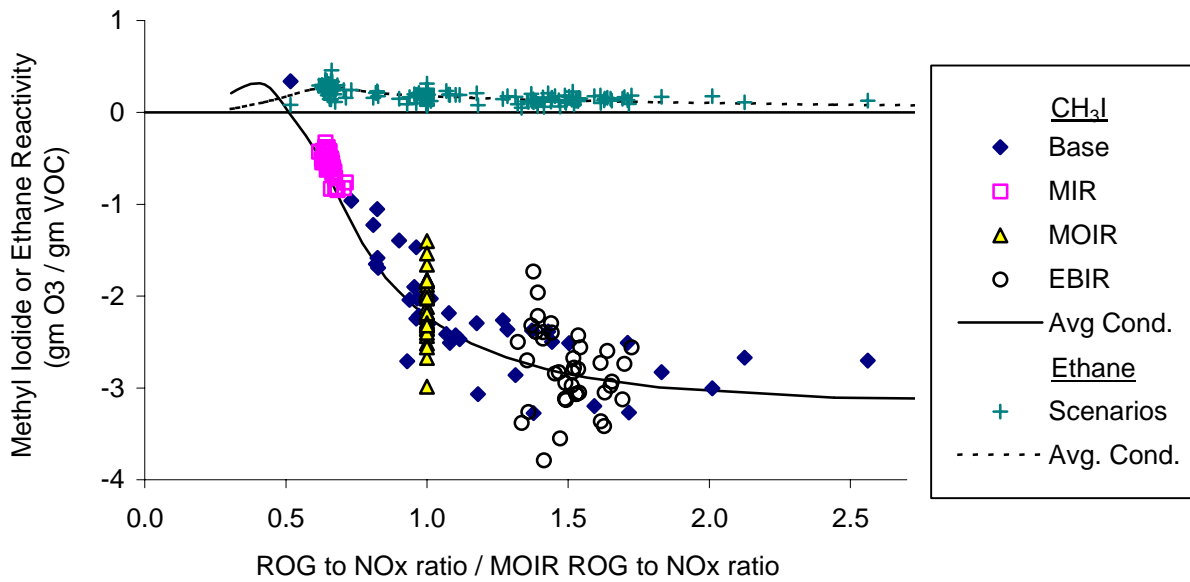


Figure 10. Plots of incremental reactivities of methyl iodide and ethane in the atmospheric reactivity scenarios against the ROG/NO_x ratio, normalized by the ROG/NO_x ratio yielding the maximum ozone concentrations.

reactivities occurring at the MIR NO_x levels, as is the case with most other VOCs. It is interesting to note that the highest incremental reactivities of methyl iodide are comparable to the highest incremental reactivities of ethane, though the NO_x conditions where it occurs are higher (the ROG/ NO_x ratios are lower). Thus, even under the very high NO_x conditions where methyl iodide has a positive impact, the magnitude of this impact is predicted not to be significantly greater than the maximum impact of ethane, the compound that has been used as the standard to define negligible reactivity for exemption purposes.

CONCLUSIONS

This project has been successful in obtaining information needed to reduce uncertainties in estimating atmospheric ozone impacts of methyl iodide, a compound that has been proposed as a potential replacement for methyl bromide in pesticide applications. A mechanism for the atmospheric reactions of methyl iodide has been developed that performs sufficiently well in simulating results of environmental chamber experiments involving methyl iodide under a variety of conditions, including those representing ozone formation in urban atmospheres at differing NO_x levels. This mechanism incorporates results of laboratory measurements of methyl iodide's absorption cross sections and OH radical rate constants, and laboratory measurements of rate constants and mechanisms for the iodine atoms and the IO radicals expected to be formed. However, uncertainties exist concerning some aspects of the mechanism, and parameters in the mechanism reflecting these uncertainties had to be adjusted to obtain model predictions that were consistent with the environmental chamber data.

The uncertainties in the methyl iodide atmospheric oxidation mechanism concern the photolysis rates of the INO_2 expected to be formed when iodine atoms react with NO_2 , and the sink processes for active iodine species, processes that are attributed to formation of I_xO_x oligomers from reactions of IO radicals. The best fits to the data are obtained if it is assumed that INO_2 photolyzes at a rate that is approximately 15 times of the calculated photolysis rate for BrNO_2 (assuming unit quantum yields), that the $\text{IO} + \text{IO}$ reaction forms I_2O_2 15% of the time, and that IO reacts with I_2O_2 or I_3O_3 to form higher oligomers with a rate constant of about $5 \times 10^{-12} \text{ cm}^3 \text{ molec}^{-1} \text{ s}^{-1}$. The possibility of compensating errors in these adjustments cannot be ruled out, though it should be noted that the mechanism simulates experiments both in the presence and absence of NO_x , suggesting that an erroneous INO_2 photolysis rate is unlikely to be compensating for errors in the iodine sink mechanisms involving IO reactions in the absence of NO_x . On the other hand, although the mechanism gives reasonably good simulations to most of the data, it does tend to underpredict the consumption of O_3 in the presence of methyl iodide that occurs at the end of some of the experiments, suggesting that the mechanism could be improved in some respects. Experimental studies of INO_2 photolysis and iodine sink reactions of IO radicals would clearly be useful in reducing these uncertainties.

In any case, the results of the experiments show that the reactions of methyl iodide can cause an increase in NO oxidation and O_3 formation rates during the initial stages of some experiments, but that it eventually causes consumption or inhibition of ozone formation. The initial enhancement of the NO oxidation and O_3 formation rates is attributed formation of methyl radicals formed in the photolysis of methyl iodide, and the eventual consumption or inhibition of O_3 is attributed to the reactions of O_3 with iodine atoms that are regenerated in chain reactions. The latter tend to be the more important in affecting overall O_3 formation under atmospheric conditions, except for conditions of very high NO_x levels.

Atmospheric reactivity calculations predict that methyl iodide will inhibit ozone formation in the atmosphere under maximum incremental reactivity (MIR), maximum ozone incremental reactivity (MOIR), equal benefit incremental reactivity (EBIR), and lower NO_x conditions. The only conditions under which methyl iodide is calculated to have a positive impact on O_3 involve higher-than-MIR NO_x levels that may occur near large NO_x sources where O_3 formation is significantly inhibited by NO and NO_2 . Most of the ambient atmosphere is characterized by the lower NO_x conditions where methyl iodide inhibits ozone formation. Even under the high NO_x conditions where methyl iodide has a positive impact, the magnitude of the impact is not much greater than that of ethane, the compound that has been used by the EPA as the standard to define negligible reactivity for the purpose of exempting VOCs from regulation as ozone precursors (Dimitriades, 1999).

Note that the mechanism developed in this work has some uncertainties, and its ability to simulate some of the experimental data could be improved. This means that there are also uncertainties in its calculated atmospheric ozone impacts, and in the conclusions that can be drawn from them. However, if the mechanism is biased, the simulations of some of the chamber data suggest that the bias is towards *underpredicting* the ozone inhibition caused by methyl iodide. Therefore, if the mechanism is in error, it is more likely than not that the actual ozone inhibition caused by methyl iodide is greater than predicted by our calculations. In this case, the conclusion that methyl iodide inhibits ozone formation under most conditions would still stand.

Therefore, we conclude that if methyl iodide emissions are to be regulated, it should be for some basis other than its effect on ground level ozone formation.

REFERENCES

- Atkinson, R. (1989): "Kinetics and Mechanisms of the Gas-Phase Reactions of the Hydroxyl Radical with Organic Compounds," J. Phys. Chem. Ref. Data, Monograph no 1.
- Baugues, K. (1990): "Preliminary Planning Information for Updating the Ozone Regulatory Impact Analysis Version of EKMA," Draft Document, Source Receptor Analysis Branch, Technical Support Division, U. S. Environmental Protection Agency, Research Triangle Park, NC, January.
- CARB (1993): "Proposed Regulations for Low-Emission Vehicles and Clean Fuels -- Staff Report and Technical Support Document," California Air Resources Board, Sacramento, CA, August 13, 1990. See also Appendix VIII of "California Exhaust Emission Standards and Test Procedures for 1988 and Subsequent Model Passenger Cars, Light Duty Trucks and Medium Duty Vehicles," as last amended September 22, 1993. Incorporated by reference in Section 1960.
- CARB (2000): "Initial Statement of Reasons for the Proposed Amendments to the Regulation for Reducing Volatile Organic Compound Emissions from Aerosol Coating Products and Proposed Tables of Maximum Incremental Reactivity (MIR) Values, and Proposed Amendments to Method 310, 'Determination of Volatile Organic Compounds in Consumer Products'," California Air Resources Board, Sacramento, CA, May 5.
- Carter, W. P. L. (1994a): "Development of Ozone Reactivity Scales for Volatile Organic Compounds," J. Air & Waste Manage. Assoc., 44, 881-899.
- Carter, W. P. L. (1994b): "Calculation of Reactivity Scales Using an Updated Carbon Bond IV Mechanism," Report Prepared for Systems Applications International Under Funding from the Auto/Oil Air Quality Improvement Research Program, April 12.
- Carter, W. P. L. (2000a): "Documentation of the SAPRC-99 Chemical Mechanism for VOC Reactivity Assessment," Report to the California Air Resources Board, Contracts 92-329 and 95-308, May 8. Available at <http://cert.ucr.edu/~carter/absts.htm#saprc99> and <http://www.cert.ucr.edu/~carter/reactdat.htm>.
- Carter, W. P. L. (2000b): "Implementation of the SAPRC-99 Chemical Mechanism into the Models-3 Framework," Report to the United States Environmental Protection Agency, January 29. Available at <http://www.cert.ucr.edu/~carter/absts.htm#s99mod3>.
- Carter, W. P. L. (2002): "Development of a Next Generation Environmental Chamber Facility for Chemical Mechanism and VOC Reactivity Research," Draft Research Plan and First Progress Report to the United States Environmental Protection Agency Cooperative Agreement CR 827331-01-0, January 3. Available at <http://www.cert.ucr.edu/~carter/epacham>.
- Carter, W. P. L. (2004): "Evaluation of a Gas-Phase Atmospheric Reaction Mechanism for Low NO_x Conditions," Final Report to California Air Resources Board Contract No. 01-305, May 5. Available at <http://www.cert.ucr.edu/~carter/absts.htm#Inoxrpt>.
- Carter, W. P. L. (2007): "Documentation of the SAPRC-07 Chemical Mechanism and Updated Ozone Reactivity Scales," Final Report to the California Air Resources Board Contract No. 03-318, June 15. Available at <http://www.cert.ucr.edu/~carter/SAPRC>.

- Carter, W. P. L. and R. Atkinson (1987): "An Experimental Study of Incremental Hydrocarbon Reactivity," *Environ. Sci. Technol.*, 21, 670-679
- Carter, W. P. L. and R. Atkinson (1989): "A Computer Modeling Study of Incremental Hydrocarbon Reactivity", *Environ. Sci. Technol.*, 23, 864.
- Carter, W. P. L., and Lurmann, F. W. (1991) Evaluation of a detailed gas-phase atmospheric reaction mechanism using environmental chamber data. *Atmos. Environ.* 25A:2771-2806.
- Carter, W. P. L., J. A. Pierce, I. L. Malkina, D. Luo and W. D. Long (1993): "Environmental Chamber Studies of Maximum Incremental Reactivities of Volatile Organic Compounds," Report to Coordinating Research Council, Project No. ME-9, California Air Resources Board Contract No. A032-0692; South Coast Air Quality Management District Contract No. C91323, United States Environmental Protection Agency Cooperative Agreement No. CR-814396-01-0, University Corporation for Atmospheric Research Contract No. 59166, and Dow Corning Corporation. April 1. Available at <http://www.cert.ucr.edu/~carter/absts.htm#rct1rept>
- Carter, W. P. L., D. Luo, I. L. Malkina, and D. Fitz (1995a): "The University of California, Riverside Environmental Chamber Data Base for Evaluating Oxidant Mechanism. Indoor Chamber Experiments through 1993," Report submitted to the U. S. Environmental Protection Agency, EPA/AREAL, Research Triangle Park, NC., March 20..
- Carter, W. P. L., D. Luo, I. L. Malkina, and J. A. Pierce (1995b): "Environmental Chamber Studies of Atmospheric Reactivities of Volatile Organic Compounds. Effects of Varying ROG Surrogate and NO_x," Final report to Coordinating Research Council, Inc., Project ME-9, California Air Resources Board, Contract A032-0692, and South Coast Air Quality Management District, Contract C91323. March 24. Available at <http://www.cert.ucr.edu/~carter/absts.htm#rct2rept>.
- Carter, W. P. L., J. H. Seinfeld, D. R. Fitz and G. S. Tonnesen (1999): "Development of a Next-Generation Environmental Chamber Facility for Chemical Mechanism and VOC Reactivity Evaluation," Research Proposal to the United States Environmental Protection Agency, February 22. (Available at <http://www.cert.ucr.edu/~carter/epacham/proposal.htm>.)
- Carter, W. P. L., D. R. Cocker III, D. R. Fitz, I. L. Malkina, K. Bumiller, C. G. Sauer, J. T. Pisano, C. Bufalino, and C. Song (2005a): "A New Environmental Chamber for Evaluation of Gas-Phase Chemical Mechanisms and Secondary Aerosol Formation", *Atmos. Environ.* 39 7768-7788.
- Carter, W. P. L. and I. L. Malkina (2005): "Evaluation of Atmospheric Impacts of Selected Coatings VOC Emissions," Final report to the California Air Resources Board Contract No. 00-333, March 15. Available at <http://www.cert.ucr.edu/~carter/absts.htm#coatpt>.
- Carter, W. P. L., D. R. Cocker III, D. R. Fitz, I. L. Malkina, K. Bumiller, C. G. Sauer, J. T. Pisano, C. Bufalino, and C. Song (2005a): "A New Environmental Chamber for Evaluation of Gas-Phase Chemical Mechanisms and Secondary Aerosol Formation", *Atmos. Environ.* 39 7768-7788.
- Carter, W. P. L., I. L. Malkina, D. R. Cocker III, and C. Song (2005b): "Environmental Chamber Studies of VOC Species in Architectural Coatings and Mobile Source Emissions," Final Report to the South Coast Air Quality Management District Contract No. 03468, July 5. Available at <http://www.cert.ucr.edu/~carter/absts.htm#scaqcham>.

- Carter, W. P. L. and I. L. Malkina (2007): "Investigation of the Atmospheric Impacts of Selected Pesticides," Final Report to the California Air Resources Board Contract 04-334, January 10. Available at <http://www.cert.ucr.edu/~carter/absts.htm#pestrep>.
- Cocker, D. R., R. C. Flagan, and J. H. Seinfeld. (2001). "State-of-the-Art Chamber Facility for Studying Atmospheric Aerosol Chemistry," *Environ. Sci. Technol.* 35, 2594-2601.
- Dimitriadis, B. (1999): "Scientific Basis of an Improved EPA Policy on Control of Organic Emissions for Ambient Ozone Reduction," *J. Air & Waste Manage. Assoc.* 49, 831-838
- IUPAC (2006): "Evaluated Kinetic and Photochemical Data". IUPAC Subcommittee on Gas Kinetic Data Evaluation for Atmospheric Chemistry. Web Version. Available at <http://www.iupac-kinetic.ch.cam.ac.uk>. Latest data sheets dated June, 2006.
- Jimenez, J. L., R. Bahreini, D. R. Cocker III, H. Zhuang, V. Varutbangkul, R. C. Flagan, J. H. Seinfeld, C. D. O'Dowd, and T. Hoffmann (2003): "New particle formation from photooxidation of diiodomethane (CH₂I₂)," *J. Geophys. Res.*, 108, 4318-4342.
- Johnson, G. M. (1983): "Factors Affecting Oxidant Formation in Sydney Air," in "The Urban Atmosphere -- Sydney, a Case Study." Eds. J. N. Carras and G. M. Johnson (CSIRO, Melbourne), pp. 393-408.
- NRC (1991): "Rethinking the Ozone Problem in Urban and Regional Air Pollution," National Research Council Committee on Tropospheric Ozone Formation and Measurement. National Academy Press, Washing, DC.
- Peterson, J. T. (1976): "Calculated Actinic Fluxes (290 - 700 nm) for Air Pollution Photochemistry Applications", EPA-600/4-76-025, June.
- Warren, B., W. P. L. Carter, Q. G. J. Malloy, and D. R. Cocker, III (2007): "An experimental and model study of the particle formation from the atmospheric reactions of methyl iodide," Manuscript in preparation.
- Zafonte, L., P. L. Rieger, and J. R. Holmes (1977): "Nitrogen Dioxide Photolysis in the Los Angeles Atmosphere," *Environ. Sci. Technol.* 11, 483-487.

APPENDIX A. BASE MECHANISM LISTING

Table A-1. List of model species used in the base SAPRC-07 mechanism, including the VOC species used in the chamber and atmospheric reactivity simulations.

Name	Description
<u>Constant Species.</u>	
O2	Oxygen
M	Air
H2O	Water
H2	Hydrogen Molecules
HV	Light
<u>Active Inorganic Species.</u>	
O3	Ozone
NO	Nitric Oxide
NO2	Nitrogen Dioxide
NO3	Nitrate Radical
N2O5	Nitrogen Pentoxide
HONO	Nitrous Acid
HNO3	Nitric Acid
HNO4	Peroxynitric Acid
HO2H	Hydrogen Peroxide
CO	Carbon Monoxide
SO2	Sulfur Dioxide
H2	Hydrogen
<u>Active Radical Species and Operators.</u>	
OH	Hydroxyl Radicals
HO2	Hydroperoxide Radicals
MEO2	Methyl Peroxy Radicals
RO2C	Peroxy Radical Operator representing NO to NO ₂ and NO ₃ to NO ₂ conversions, and the effects of peroxy radical reactions on acyl peroxy and other peroxy radicals.
RO2XC	Peroxy Radical Operator representing NO consumption (used in conjunction with organic nitrate formation), and the effects of peroxy radical reactions on NO ₃ , acyl peroxy radicals, and other peroxy radicals.
MECO3	Acetyl Peroxy Radicals
RCO3	Peroxy Propionyl and higher peroxy acyl Radicals
BZCO3	Peroxyacyl radical formed from Aromatic Aldehydes
MACO3	Peroxyacyl radicals formed from methacrolein and other acroleins.
<u>Steady State Radical Species</u>	
O3P	Ground State Oxygen Atoms
O1D	Excited Oxygen Atoms
TBUO	t-Butoxy Radicals
BZO	Phenoxy Radicals
HOCOO	Radical formed when Formaldehyde reacts with HO2

Table A-1 (continued)

Name	Description
<u>PAN and PAN Analogues</u>	
PAN	Peroxy Acetyl Nitrate
PAN2	PPN and other higher alkyl PAN analogues
PBZN	PAN analogues formed from Aromatic Aldehydes
MAPAN	PAN analogue formed from Methacrolein
<u>Explicit and Lumped Molecule Reactive Organic Product Species</u>	
HCHO	Formaldehyde
CCHO	Acetaldehyde
RCHO	Lumped C3+ Aldehydes. Mechanism based on propionaldehyde
ACET	Acetone
MEK	Ketones and other non-aldehyde oxygenated products that react with OH radicals faster than 5×10^{-13} but slower than $5 \times 10^{-12} \text{ cm}^3 \text{ molec}^{-2} \text{ sec}^{-1}$. Mechanism based on methyl ethyl ketone.
MEOH	Methanol
HCOOH	Formic Acid
CCOOH	Acetic Acid. Also used for peroxyacetic acid.
RCOOH	Higher organic acids and peroxy acids. Mechanism based on propionic acid.
COOH	Methyl Hydroperoxide
ROOH	Lumped organic hydroperoxides with 2-4 carbons. Mechanism based n-propyl hydroperoxide.
R6OOH	Lumped organic hydroperoxides with 5 or more carbons (other than those formed following OH addition to aromatic rings, which are represented separately). Mechanism based on 3-hexyl hydroperoxide.
RAOOH	Organic hydroperoxides formed following OH addition to aromatic rings, which is represented separately because of their probable role in SOA formation. Mechanism based on two isomers expected to be formed in the m-xylene system.
GLY	Glyoxal
MGLY	Methyl Glyoxal
BACL	Biacetyl
CRES	Phenols and Cresols. Mechanism based on o-cresol.
NPHE	Nitrophenols
BALD	Aromatic aldehydes. Mechanism based on benzaldehyde
MACR	Methacrolein
MVK	Methyl Vinyl Ketone
IPRD	Lumped isoprene product species. Mechanism based on that of Carter and Atkinson (1996).
<u>Aromatic unsaturated ring fragmentation products (see discussion of aromatic mechanisms)</u>	
AFG1	Lumped photoreactive monounsaturated dicarbonyl aromatic fragmentation products that photolyze to form radicals.
AFG2	Lumped photoreactive monounsaturated dicarbonyl aromatic fragmentation products that photolyze to form non-radical products
AFG3	Lumped diunsaturated dicarbonyl aromatic fragmentation product.

Table A-1 (continued)

Name	Description
<u>Lumped Parameter Products</u>	
PROD2	Ketones and other non-aldehyde oxygenated products that react with OH radicals faster than $5 \times 10^{-12} \text{ cm}^3 \text{ molec}^{-2} \text{ sec}^{-1}$. Mechanism based on $\text{CH}_3\text{C}(\text{O})\text{CH}_2\text{CH}_2\text{CH}_2\text{OH}$, $\text{CH}_3\text{C}(\text{O})\text{CH}_2\text{CH}(\text{CH}_3)\text{CH}_2\text{OH}$, $\text{CH}_3\text{CH}_2\text{C}(\text{O})\text{CH}_2\text{CH}_2\text{CH}(\text{CH}_3)\text{OH}$, $\text{CH}_3\text{CH}_2\text{C}(\text{O})\text{CH}_2\text{CH}_2\text{CH}(\text{OH})\text{CH}_2\text{CH}_3$, and $\text{CH}_3\text{CH}_2\text{CH}_2\text{CH}(\text{OH})\text{CH}_2\text{CH}_2\text{C}(\text{O})\text{CH}_2\text{CH}_3$ (PROD2-1 through 5), each weighed equally.
RNO3	Lumped Organic Nitrates. Mechanism based on $\text{CH}_3\text{CH}_2\text{CH}(\text{CH}_3)\text{ONO}_2$, $\text{CH}_3\text{CH}(\text{OH})\text{CH}_2\text{CH}_2\text{CH}_2\text{ONO}_2$, $\text{CH}_3\text{CH}_2\text{CH}(\text{CH}_3)\text{CH}(\text{CH}_3)\text{ONO}_2$, $\text{CH}_3\text{CH}_2\text{CH}_2\text{CH}_2\text{CH}_2\text{CH}(\text{ONO}_2)\text{CH}_2\text{OH}$, $\text{CH}_3\text{CH}_2\text{C}(\text{CH}_3)(\text{ONO}_2)\text{CH}_2\text{CH}(\text{CH}_3)\text{CH}_3$, and $\text{CH}_3\text{CH}_2\text{CH}_2\text{CH}_2\text{CH}_2\text{CH}_2\text{CH}_2\text{CH}(\text{ONO}_2)\text{CH}_2\text{CH}_3$ (RNO3-1 through 6), each weighed equally.
<u>Steady state operators used to represent radical or product formation in peroxy radical reactions.</u>	
xHO2	Formation of HO_2 from alkoxy radicals formed in peroxy radical reactions with NO and NO_3 (100% yields) and RO_2 (50% yields)
xOH	As above, but for OH
xNO2	As above, but for NO_2
xMEO2	As above, but for MEO2
xMECO3	As above, but for MECO3
xRCO3	As above, but for RCO3
xMACO3	As above, but for MACO3
xTBUO	As above, but for TBUO
xCO	As above, but for CO
xHNO3	As above, but for HNO3
xHCHO	As above, but for HCHO
xCCHO	As above, but for CCHO
xRCHO	As above, but for RCHO
xACET	As above, but for ACET
xMEK	As above, but for MEK
xPROD2	As above, but for PROD2
xGLY	As above, but for GLY
xMGLY	As above, but for MGLY
xBACL	As above, but for BACL
xBALD	As above, but for BALD
xAFG1	As above, but for AFG1
xAFG2	As above, but for AFG2
xAFG3	As above, but for AFG3
xMACR	As above, but for MACR
xMVK	As above, but for MVK
xIPRD	As above, but for IPRD
xRNO3	As above, but for RNO3
xHCOOH	As above, but for HCOOH
xCCOOH	As above, but for CCOOH
xRCOOH	As above, but for RCOOH
zRNO3	Formation of RNO3 in the $\text{RO}_2 + \text{NO}$, reaction, or formation of corresponding non-nitrate products (represented by PROD2) formed from alkoxy radicals formed in $\text{RO}_2 + \text{NO}_3$ and (in 50% yields) $\text{RO}_2 + \text{RO}_2$ reactions.

Table A-1 (continued)

Name	Description
yROOH	Formation of ROOH following $RO_2 + HO_2$ reactions, or formation of H-shift disproportionation products (represented by MEK) in the $RO_2 + RCO_3$ and (in 50% yields) $RO_2 + RO_2$ reactions.
yR6OOH	As above, but with the $RO_2 + HO_2$ product represented by R6OOH and the H-shift products are represented by PROD2.
yRAOOH	As above, but with the $RO_2 + HO_2$ product represented by R6OOH
<u>Non-Reacting Species</u>	
CO2	Carbon Dioxide
SULF	Sulfates (SO_3 or H_2SO_4)
XC	Lost Carbon or carbon in unreactive products
XN	Lost Nitrogen or nitrogen in unreactive products
<u>Primary Organics Represented explicitly</u>	
CH4	Methane
ETHENE	Ethene
ISOPRENE	Isoprene
ACETYLEN	Acetylene
BENZENE	Benzene
Organics represented explicitly in the chamber simulations (not used in the atmospheric simulations)	
N-C4	n-Butane
N-C6	n-Hexane
N-C8	n-Octane
PROPENE	Propene
T-2-BUTE	trans-2-Butene
TOLUENE	Toluene
M-XYLENE	m-Xylene
<u>Lumped model species used in the atmospheric reactivity simulations (not used in chamber simulations)</u>	
ALK1	Alkanes and other non-aromatic compounds that react only with OH, and have kOH (OH radical rate constant) between 2 and $5 \times 10^2 \text{ ppm}^{-1} \text{ min}^{-1}$. (Primarily ethane)
ALK2	Alkanes and other non-aromatic compounds that react only with OH, and have kOH between 5×10^2 and $2.5 \times 10^3 \text{ ppm}^{-1} \text{ min}^{-1}$. (Primarily propane)
ALK3	Alkanes and other non-aromatic compounds that react only with OH, and have kOH between 2.5×10^3 and $5 \times 10^3 \text{ ppm}^{-1} \text{ min}^{-1}$.
ALK4	Alkanes and other non-aromatic compounds that react only with OH, and have kOH between 5×10^3 and $1 \times 10^4 \text{ ppm}^{-1} \text{ min}^{-1}$.
ALK5	Alkanes and other non-aromatic compounds that react only with OH, and have kOH greater than $1 \times 10^4 \text{ ppm}^{-1} \text{ min}^{-1}$.
ARO1	Aromatics with $kOH < 2 \times 10^4 \text{ ppm}^{-1} \text{ min}^{-1}$.
ARO2	Aromatics with $kOH > 2 \times 10^4 \text{ ppm}^{-1} \text{ min}^{-1}$.
OLE1	Alkenes (other than ethene) with $kOH < 7 \times 10^4 \text{ ppm}^{-1} \text{ min}^{-1}$.
OLE2	Alkenes with $kOH > 7 \times 10^4 \text{ ppm}^{-1} \text{ min}^{-1}$.
TERP	Terpenes

Table A-2. Reactions and rate constants in the base SAPRC-07 mechanism used in this work. See Carter (2007) for documentation.

Label	Reaction and Products [a]	Rate Parameters [b]			
		k(300)	A	Ea	B
Inorganic Reactions					
1	NO ₂ + HV = NO + O ₃ P		Phot Set= NO2-06		
2	O ₃ P + O ₂ + M = O ₃ + M	5.68e-34	5.68e-34	0.00	-2.60
3	O ₃ P + O ₃ = #2 O ₂	8.34e-15	8.00e-12	4.09	
4	O ₃ P + NO = NO ₂	1.64e-12	Falloff, F=0.60, N=1.00		
		0:	9.00e-32	0.00	-1.50
		inf:	3.00e-11	0.00	0.00
5	O ₃ P + NO ₂ = NO + O ₂	1.03e-11	5.50e-12	-0.37	
6	O ₃ P + NO ₂ = NO ₃	3.24e-12	Falloff, F=0.60, N=1.00		
		0:	2.50e-31	0.00	-1.80
		inf:	2.20e-11	0.00	-0.70
7	O ₃ + NO = NO ₂ + O ₂	2.02e-14	3.00e-12	2.98	
8	O ₃ + NO ₂ = O ₂ + NO ₃	3.72e-17	1.40e-13	4.91	
9	NO + NO ₃ = #2 NO ₂	2.60e-11	1.80e-11	-0.22	
10	NO + NO + O ₂ = #2 NO ₂	1.93e-38	3.30e-39	-1.05	
11	NO ₂ + NO ₃ = N ₂ O ₅	1.24e-12	Falloff, F=0.35, N=1.33		
		0:	3.60e-30	0.00	-4.10
		inf:	1.90e-12	0.00	0.20
12	N ₂ O ₅ = NO ₂ + NO ₃	5.69e-2	Falloff, F=0.35, N=1.33		
		0:	1.30e-3	21.86	-3.50
		inf:	9.70e+14	22.02	0.10
13	N ₂ O ₅ + H ₂ O = #2 HNO ₃	2.50e-22			
14	N ₂ O ₅ + H ₂ O + H ₂ O = #2 HNO ₃ + H ₂ O	1.80e-39			
	N ₂ O ₅ + HV = NO ₃ + NO + O ₃ P		(Slow)		
	N ₂ O ₅ + HV = NO ₃ + NO ₂		(Slow)		
15	NO ₂ + NO ₃ = NO + NO ₂ + O ₂	6.75e-16	4.50e-14	2.50	
16	NO ₃ + HV = NO + O ₂		Phot Set= NO3NO-06		
17	NO ₃ + HV = NO ₂ + O ₃ P		Phot Set= NO3NO2-6		
18	O ₃ + HV = O ₁ D + O ₂		Phot Set= O3O1D-06		
19	O ₃ + HV = O ₃ P + O ₂		Phot Set= O3O3P-06		
20	O ₁ D + H ₂ O = #2 OH	1.99e-10			
21	O ₁ D + M = O ₃ P + M	3.28e-11	2.38e-11	-0.19	
22	OH + NO = HONO	7.31e-12	Falloff, F=0.60, N=1.00		
		0:	7.00e-31	0.00	-2.60
		inf:	3.60e-11	0.00	-0.10
23	HONO + HV = OH + NO		Phot Set= HONO-06		
24	OH + HONO = H ₂ O + NO ₂	5.95e-12	2.50e-12	-0.52	
25	OH + NO ₂ = HNO ₃	1.05e-11	Falloff, F=0.60, N=1.00		
		0:	1.80e-30	0.00	-3.00
		inf:	2.80e-11	0.00	0.00
26	OH + NO ₃ = HO ₂ + NO ₂	2.00e-11			

Table A-2 (continued)

Label	Reaction and Products [a]	Rate Parameters [b]			
		k(300)	A	Ea	B
27	OH + HNO3 = H2O + NO3	1.51e-13	k = k0+k3M/(1+k3M/k2)		
			k0: 2.40e-14	-0.91	0.00
			k2: 2.70e-17	-4.37	0.00
			k3: 6.50e-34	-2.65	0.00
28	HNO3 + HV = OH + NO2		Phot Set= HNO3		
29	OH + CO = HO2 + CO2	2.28e-13	k = k1 + k2 [M]		
			k1: 1.44e-13	0.00	0.00
			k2: 3.43e-33	0.00	0.00
30	OH + O3 = HO2 + O2	7.41e-14	1.70e-12	1.87	
31	HO2 + NO = OH + NO2	8.85e-12	3.60e-12	-0.54	
32	HO2 + NO2 = HNO4	1.12e-12	Falloff, F=0.60, N=1.00		
			0: 2.00e-31	0.00	-3.40
			inf: 2.90e-12	0.00	-1.10
33	HNO4 = HO2 + NO2	1.07e-1	Falloff, F=0.60, N=1.00		
			0: 3.72e-5	21.16	-2.40
			inf: 5.42e+15	22.20	-2.30
34	HNO4 + HV = #.61 {HO2 + NO2} + #.39 {OH + NO3}		Phot Set= HNO4-06		
35	HNO4 + OH = H2O + NO2 + O2	4.61e-12	1.30e-12	-0.76	
36	HO2 + O3 = OH + #2 O2	1.69e-15	2.03e-16	-1.26	4.57
37	HO2 + HO2 = HO2H + O2	2.84e-12	k = k1 + k2 [M]		
			k1: 2.20e-13	-1.19	0.00
			k2: 1.90e-33	-1.95	0.00
38	HO2 + HO2 + H2O = HO2H + O2 + H2O	6.09e-30	k = k1 + k2 [M]		
			k1: 3.08e-34	-5.56	0.00
			k2: 2.66e-54	-6.32	0.00
39	NO3 + HO2 = #.8 {OH + NO2 + O2} + #.2 {HNO3 + O2}	4.00e-12			
40	NO3 + NO3 = #2 NO2 + O2	2.41e-16	8.50e-13	4.87	
41	HO2H + HV = #2 OH		Phot Set= H2O2		
42	HO2H + OH = HO2 + H2O	1.80e-12	1.80e-12	0.00	
43	OH + HO2 = H2O + O2	1.10e-10	4.80e-11	-0.50	
44	OH + SO2 = HO2 + SULF	9.49e-13	Falloff, F=0.60, N=1.00		
			0: 3.30e-31	0.00	-4.30
			inf: 1.60e-12	0.00	0.00
45	OH + H2 = HO2 + H2O	7.02e-15	7.70e-12	4.17	
<u>Methyl peroxy and methoxy reactions</u>					
BR01	MEO2 + NO = NO2 + HCHO + HO2	7.64e-12	2.30e-12	-0.72	
BR02	MEO2 + HO2 = COOH + O2	4.65e-12	3.46e-13	-1.55	0.36
BR03	MEO2 + HO2 = HCHO + O2 + H2O	4.50e-13	3.34e-14	-1.55	-3.53
BR04	MEO2 + NO3 = HCHO + HO2 + NO2	1.30e-12			
BR05	MEO2 + MEO2 = MEOH + HCHO + O2	2.16e-13	6.39e-14	-0.73	-1.80
BR06	MEO2 + MEO2 = #2 {HCHO + HO2}	1.31e-13	7.40e-13	1.03	
<u>Active Peroxy Radical Operators</u>					
BR07	RO2C + NO = NO2	9.23e-12	2.60e-12	-0.76	
BR08	RO2C + HO2 = HO2	7.63e-12	3.80e-13	-1.79	

Table A-2 (continued)

Label	Reaction and Products [a]	Rate Parameters [b]			
		k(300)	A	Ea	B
BR09	RO2C + NO3 = NO2	2.30e-12			
BR10	RO2C + MEO2 = #.5 {RO2C + xHO2 + xHCHO + O2} + #.25 {HCHO + MEOH}	2.00e-13			
BR11	RO2C + RO2C =	3.50e-14			
BR12	RO2XC + NO = XN		Same k as rxn BR07		
BR13	RO2XC + HO2 = HO2		Same k as rxn BR08		
BR14	RO2XC + NO3 = NO2		Same k as rxn BR09		
BR15	RO2XC + MEO2 = #.5 {RO2C + xHO2 + xHCHO + O2} + #.25 {HCHO + MEOH}		Same k as rxn BR10		
BR16	RO2XC + RO2C =		Same k as rxn BR11		
BR17	RO2XC + RO2XC =		Same k as rxn BR11		
<u>Reactions of Acyl Peroxy Radicals, PAN, and PAN analogues</u>					
BR18	MECO3 + NO2 = PAN	9.37e-12	Falloff, F=0.30, N=1.41 0: 2.70e-28 0.00 -7.10 inf: 1.21e-11 0.00 -0.90		
BR19	PAN = MECO3 + NO2	6.27e-4	Falloff, F=0.30, N=1.41 0: 4.90e-3 24.05 0.00 inf: 4.00e+16 27.03 0.00		
BR20	PAN + HV = #.6 {MECO3 + NO2} + #.4 {MEO2 + CO2 + NO3}		Phot Set= PAN		
BR21	MECO3 + NO = MEO2 + CO2 + NO2	1.97e-11	7.50e-12	-0.58	
BR22	MECO3 + HO2 = CCOOH + #.7 O2 + #.3 O3	1.36e-11	5.20e-13	-1.95	
BR23	MECO3 + NO3 = MEO2 + CO2 + NO2 + O2		Same k as rxn BR09		
BR24	MECO3 + MEO2 = #.9 {CCOOH + HCHO + O2} + #.1 {HCHO + HO2 + MEO2 + CO2}	1.06e-11	2.00e-12	-0.99	
BR25	MECO3 + RO2C = CCOOH	1.56e-11	4.40e-13	-2.13	
BR26	MECO3 + RO2XC = CCOOH		Same k as rxn BR25		
BR27	MECO3 + MECO3 = #2 {MEO2 + CO2} + O2	1.54e-11	2.90e-12	-0.99	
BR28	RCO3 + NO2 = PAN2	1.21e-11	1.21e-11	0.00	-1.07
BR29	PAN2 = RCO3 + NO2	5.48e-4	8.30e+16	27.70	
BR30	RCO3 + NO = NO2 + RO2C + xHO2 + yROOH + xCCHO + CO2	2.08e-11	6.70e-12	-0.68	
BR31	RCO3 + HO2 = RCOOH + #.75 O2 + #.25 O3		Same k as rxn BR22		
BR32	RCO3 + NO3 = NO2 + RO2C + xHO2 + yROOH + xCCHO + CO2 + O2		Same k as rxn BR09		
BR33	RCO3 + MEO2 = RCOOH + HCHO + O2		Same k as rxn BR24		
BR34	RCO3 + RO2C = RCOOH + O2		Same k as rxn BR25		
BR35	RCO3 + RO2XC = RCOOH + O2		Same k as rxn BR25		
BR36	RCO3 + MECO3 = #2 CO2 + MEO2 + RO2C + xHO2 + yROOH + xCCHO + O2		Same k as rxn BR27		
BR37	RCO3 + RCO3 = #2 {RO2C + xHO2 + xCCHO + yROOH + CO2}		Same k as rxn BR27		
BR38	BZCO3 + NO2 = PBZN	1.37e-11			
BR39	PBZN = BZCO3 + NO2	4.27e-4	7.90e+16	27.82	
BR40	BZCO3 + NO = NO2 + CO2 + BZO + RO2C		Same k as rxn BR30		

Table A-2 (continued)

Label	Reaction and Products [a]	Rate Parameters [b]			
		k(300)	A	Ea	B
BR41	BZCO3 + HO2 = RCOOH + #.75 O2 + #.25 O3 + #4 XC	Same k as rxn BR22			
BR42	BZCO3 + NO3 = NO2 + CO2 + BZO + RO2C + O2	Same k as rxn BR09			
BR43	BZCO3 + MEO2 = RCOOH + HCHO + O2 + #4 XC	Same k as rxn BR24			
BR44	BZCO3 + RO2C = RCOOH + O2 + #4 XC	Same k as rxn BR25			
BR45	BZCO3 + RO2XC = RCOOH + O2 + #4 XC	Same k as rxn BR25			
BR46	BZCO3 + MECO3 = #2 CO2 + MEO2 + BZO + RO2C	Same k as rxn BR27			
BR47	BZCO3 + RCO3 = #2 CO2 + RO2C + xHO2 + yROOH + xCCHO + BZO + RO2C	Same k as rxn BR27			
BR48	BZCO3 + BZCO3 = #2 {BZO + RO2C + CO2}	Same k as rxn BR27			
BR49	MACO3 + NO2 = MAPAN	Same k as rxn BR28			
BR50	MAPAN = MACO3 + NO2	4.79e-4	1.60e+16	26.80	
BR51	MACO3 + NO = NO2 + CO2 + HCHO + MECO3	Same k as rxn BR30			
BR52	MACO3 + HO2 = RCOOH + #.75 O2 + #.25 O3 + XC	Same k as rxn BR22			
BR53	MACO3 + NO3 = NO2 + CO2 + HCHO + MECO3 + O2	Same k as rxn BR09			
BR54	MACO3 + MEO2 = RCOOH + HCHO + XC + O2	Same k as rxn BR24			
BR55	MACO3 + RO2C = RCOOH + XC	Same k as rxn BR25			
BR56	MACO3 + RO2XC = RCOOH + O2 + XC	Same k as rxn BR25			
BR57	MACO3 + MECO3 = #2 CO2 + MEO2 + HCHO + MECO3 + O2	Same k as rxn BR27			
BR58	MACO3 + RCO3 = HCHO + MECO3 + RO2C + xHO2 + yROOH + xCCHO + #2 CO2	Same k as rxn BR27			
BR59	MACO3 + BZCO3 = HCHO + MECO3 + BZO + RO2C + #2 CO2	Same k as rxn BR27			
BR60	MACO3 + MACO3 = #2 {HCHO + MECO3 + CO2}	Same k as rxn BR27			
<u>Other Organic Radical Species</u>					
BR61	TBUO + NO2 = RNO3 + #-2 XC	2.40e-11			
BR62	TBUO = ACET + MEO2	1.18e+3	7.50e+14	16.20	
BR63	BZO + NO2 = NPHE	3.79e-11	2.30e-11	-0.30	
BR64	BZO + HO2 = CRES + #-1 XC	Same k as rxn BR08			
BR65	BZO = CRES + RO2C + xHO2 + #-1 XC	1.00e-3			
<u>Steady-State Peroxy Radical operators (for formation of inorganic and radical products) [c]</u>					
RO01	xHO2 = HO2	k is variable parameter: RO2RO			
RO02	xHO2 =	k is variable parameter: RO2XRO			
RO03	xOH = OH	k is variable parameter: RO2RO			
RO04	xOH =	k is variable parameter: RO2XRO			
RO05	xNO2 = NO2	k is variable parameter: RO2RO			
RO06	xNO2 = XN	k is variable parameter: RO2XRO			
RO07	xMEO2 = MEO2	k is variable parameter: RO2RO			
RO08	xMEO2 = XC	k is variable parameter: RO2XRO			
RO09	xMECO3 = MECO3	k is variable parameter: RO2RO			
RO10	xMECO3 = #2 XC	k is variable parameter: RO2XRO			
RO11	xRCO3 = RCO3	k is variable parameter: RO2RO			
RO12	xRCO3 = #3 XC	k is variable parameter: RO2XRO			
RO13	xMACO3 = MACO3	k is variable parameter: RO2RO			

Table A-2 (continued)

Label	Reaction and Products [a]	Rate Parameters [b]			
		k(300)	A	Ea	B
RO14	xMACO3 = #4 XC	k is variable parameter: RO2XRO			
RO15	xTBUO = TBUO	k is variable parameter: RO2RO			
RO16	xTBUO = #4 XC	k is variable parameter: RO2XRO			
RO17	xCO = CO	k is variable parameter: RO2RO			
RO18	xCO = XC	k is variable parameter: RO2XRO			
RO19	xHNO3 = HNO3	k is variable parameter: RO2RO			
RO20	xHNO3 = XN	k is variable parameter: RO2XRO			
<u>Explicit and Lumped Molecule Organic Products</u>					
BP01	HCHO + HV = #2 HO2 + CO	Phot Set= HCHOR-06			
BP02	HCHO + HV = H2 + CO	Phot Set= HCHOM-06			
BP03	HCHO + OH = HO2 + CO + H2O	8.47e-12	5.40e-12	-0.27	
BP04	HCHO + HO2 = HOCOO	7.79e-14	9.70e-15	-1.24	
BP05	HOCOO = HO2 + HCHO	1.76e+2	2.40e+12	13.91	
BP06	HOCOO + NO = HCOOH + NO2 + HO2	Same k as rxn BR01			
BP07	HCHO + NO3 = HNO3 + HO2 + CO	6.06e-16	2.00e-12	4.83	
BP08	CCHO + OH = MECO3 + H2O	1.49e-11	4.40e-12	-0.73	
BP09	CCHO + HV = CO + HO2 + MEO2	Phot Set= CCHO_R			
BP10	CCHO + NO3 = HNO3 + MECO3	2.84e-15	1.40e-12	3.70	
BP11	RCHO + OH = #.965 RCO3 + #.035 {RO2C + xHO2 + xCO + xCCHO + yROOH}	1.97e-11	5.10e-12	-0.80	
BP12	RCHO + HV = RO2C + xHO2 + yROOH + xCCHO + CO + HO2	Phot Set= C2CHO			
BP13	RCHO + NO3 = HNO3 + RCO3	6.74e-15	1.40e-12	3.18	
BP14	ACET + OH = RO2C + xMECO3 + xHCHO + yROOH	1.91e-13	4.56e-14	-0.85	3.65
BP15	ACET + HV = #.62 MECO3 + #1.38 MEO2 + #.38 CO	Phot Set= ACET-06, qy= 0.5			
BP16	MEK + OH = #.967 RO2C + #.039 {RO2XC + zRNO3} + #.376 xHO2 + #.51 xMECO3 + #.074 xRCO3 + #.088 xHCHO + #.504 xCCHO + #.376 xRCHO + yROOH + #.3 XC	1.20e-12	1.30e-12	0.05	2.00
BP17	MEK + HV = MECO3 + RO2C + xHO2 + xCCHO + yROOH	Phot Set= MEK-06, qy= 0.175			
BP18	MEOH + OH = HCHO + HO2	9.02e-13	2.85e-12	0.69	
BP19	HCOOH + OH = HO2 + CO2	4.50e-13			
BP20	CCOOH + OH = #.509 MEO2 + #.491 RO2C + #.509 CO2 + #.491 xHO2 + #.491 xMGLY + #.491 yROOH + #-.0.491 XC	7.26e-13	4.20e-14	-1.70	
BP21	RCOOH + OH = RO2C + #.08 CO2 + xHO2 + #.063 CO2 + #.142 xCCHO + #.4 xRCHO + #.457 xBACL + yROOH + #-.0.455 XC	1.20e-12			
BP22	COOH + OH = H2O + #.35 {HCHO + OH} + #.65 MEO2	5.46e-12	2.90e-12	-0.38	
BP23	COOH + HV = HCHO + HO2 + OH	Phot Set= COOH			

Table A-2 (continued)

Label	Reaction and Products [a]	Rate Parameters [b]			
		k(300)	A	Ea	B
BP24	ROOH + OH = #.659 OH + #.339 RO2C + #.003 RO2XC + #.003 zRNO3 + #.659 RCHO + #.045 xOH + #.293 xHO2 + #.046 xHCHO + #.045 xCCHO + #.168 xRCHO + #.125 xMEK + #.341 yROOH + #-0.135 XC	6.78e-12			
BP25	ROOH + HV = RCHO + HO2 + OH		Phot Set= COOH		
BP26	R6OOH + OH = #.691 OH + #.395 RO2C + #.046 {RO2XC + zRNO3} + #.691 PROD2 + #.151 xOH + #.112 xHO2 + #.062 xCCHO + #.235 xRCHO + #.112 xPROD2 + #.309 yR6OOH + #.077 XC	1.64e-11			
BP27	R6OOH + HV = OH + #.142 HO2 + #.782 RO2C + #.077 RO2XC + #.077 zRNO3 + #.085 RCHO + #.142 PROD2 + #.782 xHO2 + #.026 xCCHO + #.058 xRCHO + #.698 xPROD2 + #.858 yR6OOH + #.017 XC		Phot Set= COOH		
BP28	RAOOH + OH = #.045 OH + #.192 HO2 + #.630 RO2C + #.132 {RO2XC + zRNO3} + #.1 PROD2 + #.093 MGLY + #.045 IPRD + #.032 xOH + #.598 xHO2 + #.594 xRCHO + #.021 xMEK + #.205 xMGLY + #.021 xAFG1 + #.021 xAFG2 + #.763 yR6OOH + #3.413 XC	1.08e-10			
BP29	RAOOH + HV = OH + HO2 + #.5 {GLY + MGLY + AFG1 + AFG2} + #.5 XC		Phot Set= COOH		
BP30	GLY + HV = #2 {CO + HO2}		Phot Set= GLY-07R		
BP31	GLY + HV = HCHO + CO		Phot Set= GLY-07M		
BP32	GLY + OH = #.63 HO2 + #1.26 CO + #.37 RCO3 + #- .37 XC	1.10e-11			
BP33	GLY + NO3 = HNO3 + #.63 HO2 + #1.26 CO + #.37 RCO3 + #-0.37 XC	1.02e-15	2.80e-12	4.72	
BP34	MGLY + HV = HO2 + CO + MECO3		Phot Set= MGLY-06		
BP35	MGLY + OH = CO + MECO3	1.50e-11			
BP36	MGLY + NO3 = HNO3 + CO + MECO3	2.53e-15	1.40e-12	3.77	
BP37	BACL + HV = #2 MECO3		Phot Set= BACL-07		
BP38	CRES + OH = #.2 BZO + #.8 {RO2C + xHO2 + yR6OOH} + #.25 xMGLY + #5.05 XC	4.03e-11	1.70e-12	-1.89	
BP39	CRES + NO3 = HNO3 + BZO + XC	1.40e-11			
BP40	NPHE + OH = BZO + XN	3.50e-12			
BP41	NPHE + HV = HONO + #6 XC		Phot Set= NO2-06, qy= 1.5e-3		
BP42	NPHE + HV = #6 XC + XN		Phot Set= NO2-06, qy= 1.5e-2		
BP43	BALD + OH = BZCO3	1.20e-11			
BP44	BALD + HV = #7 XC		Phot Set= BALD-06, qy= 0.06		
BP45	BALD + NO3 = HNO3 + BZCO3	2.73e-15	1.34e-12	3.70	

Table A-2 (continued)

Label	Reaction and Products [a]	Rate Parameters [b]			
		k(300)	A	Ea	B
<u>Lumped Unsaturated Aromatic Ring-Opening Products</u>					
BP46	AFG1 + OH = #.217 MACO3 + #.723 RO2C + #.060 {RO2XC + zRNO3} + #.060 zRNO3 + #.521 xHO2 + #.201 xMECO3 + #.334 xCO + #.407 xRCHO + #.129 xMEK + #.107 xGLY + #.267 xMGLY + #.783 yR6OOH + #-0.76 XC	7.40e-11			
BP47	AFG1 + O3 = #.826 OH + #.522 HO2 + #.652 RO2C + #.522 CO + #.174 CO2 + #.432 GLY + #.568 MGLY + #.652 xRCO3 + #.652 xHCHO + #.652 yR6OOH + #-0.872 XC	9.66e-18			
BP48	AFG1 + HV = #1.023 HO2 + #.173 MEO2 + #.305 MECO3 + #.500 MACO3 + #.695 CO + #.195 GLY + #.305 MGLY + #.217 XC				Phot Set= AFG1
BP49	AFG2 + OH = #.217 MACO3 + #.723 RO2C + #.060 {RO2XC + zRNO3} + #.060 zRNO3 + #.521 xHO2 + #.201 xMECO3 + #.334 xCO + #.407 xRCHO + #.129 xMEK + #.107 xGLY + #.267 xMGLY + #.783 yR6OOH + #-0.76 XC	7.40e-11			
BP50	AFG2 + O3 = #.826 OH + #.522 HO2 + #.652 RO2C + #.522 CO + #.174 CO2 + #.432 GLY + #.568 MGLY + #.652 xRCO3 + #.652 xHCHO + #.652 yR6OOH + #-0.872 XC	9.66e-18			
BP51	AFG2 + HV = PROD2 + #-1 XC				Phot Set= AFG1
BP52	AFG3 + OH = #.206 MACO3 + #.733 RO2C + #.117 {RO2XC + zRNO3} + #.117 zRNO3 + #.561 xHO2 + #.117 xMECO3 + #.114 xCO + #.274 xGLY + #.153 xMGLY + #.019 xBACL + #.195 xAFG1 + #.195 xAFG2 + #.231 xIPRD + #.794 yR6OOH + #.236 XC	9.35e-11			
BP53	AFG3 + O3 = #.471 OH + #.554 HO2 + #.013 MECO3 + #.258 RO2C + #.007 {RO2XC + zRNO3} + #.007 zRNO3 + #.580 CO + #.190 CO2 + #.366 GLY + #.184 MGLY + #.350 AFG1 + #.350 AFG2 + #.139 AFG3 + #.003 MACR + #.004 MVK + #.003 IPRD + #.095 xHO2 + #.163 xRCO3 + #.163 xHCHO + #.095 xMGLY + #.264 yR6OOH + #-0.617 XC	1.43e-17			
BP54	MACR + OH = #.5 MACO3 + #.5 {RO2C + xHO2} + #.416 xCO + #.084 xHCHO + #.416 xMEK + #.084 xMGLY + #.5 yROOH + #-0.416 XC	2.84e-11	8.00e-12	-0.76	
BP55	MACR + O3 = #.208 OH + #.108 HO2 + #.1 RO2C + #.45 CO + #.117 CO2 + #.1 HCHO + #.9 MGLY + #.333 HCOOH + #.1 xRCO3 + #.1 xHCHO + #.1 yROOH + #-0.1 XC	1.28e-18	1.40e-15	4.17	
BP56	MACR + NO3 = #.5 {MACO3 + RO2C + HNO3 + xHO2 + xCO} + #.5 yROOH + #1.5 XC + #.5 XN	3.54e-15	1.50e-12	3.61	
BP57	MACR + O3P = RCHO + XC	6.34e-12			

Table A-2 (continued)

Label	Reaction and Products [a]	Rate Parameters [b]			
		k(300)	A	Ea	B
BP58	MACR + HV = #.33 OH + #.67 HO2 + #.34 MECO3 + #.33 MACO3 + #.33 RO2C + #.67 CO + #.34 HCHO + #.33 xMECO3 + #.33 xHCHO + #.33 yROOH	Phot Set= MACR-06			
BP59	MVK + OH = #.975 RO2C + #.025 {RO2XC + zRNO3} + #.3 xHO2 + #.675 xMECO3 + #.3 xHCHO + #.675 xRCHO + #.3 xMGLY + yROOH + #-.0.725 XC	1.99e-11	2.60e-12	-1.21	
BP60	MVK + O3 = #.164 OH + #.064 HO2 + #.05 {RO2C + xHO2} + #.475 CO + #.124 CO2 + #.05 HCHO + #.95 MGLY + #.351 HCOOH + #.05 xRCO3 + #.05 xHCHO + #.05 yROOH + #-.0.05 XC	5.36e-18	8.50e-16	3.02	
BP61	MVK + NO3 = #4 XC + XN		(Slow)		
BP62	MVK + O3P = #.45 RCHO + #.55 MEK + #.45 XC	4.32e-12			
BP63	MVK + HV = #.4 MEO2 + #.6 CO + #.6 PROD2 + #.4 MACO3 + #-.2.2 XC	Phot Set= MVK-06			
BP64	IPRD + OH = #.289 MACO3 + #.67 {RO2C + xHO2} + #.041 {RO2XC + zRNO3} + #.336 xCO + #.055 xHCHO + #.129 xCCHO + #.013 xRCHO + #.15 xMEK + #.332 xPROD2 + #.15 xGLY + #.174 xMGLY + #-.0.504 XC + #.711 yR6OOH	6.19e-11			
BP65	IPRD + O3 = #.285 OH + #.4 HO2 + #.048 {RO2C + xRCO3} + #.498 CO + #.14 CO2 + #.124 HCHO + #.21 MEK + #.023 GLY + #.742 MGLY + #.1 HCOOH + #.372 RCOOH + #.047 xCCHO + #.001 xHCHO + #.048 yR6OOH + #-.329 XC	4.18e-18			
BP66	IPRD + NO3 = #.15 {MACO3 + HNO3} + #.799 {RO2C + xHO2} + #.051 {RO2XC + zRNO3} + #.572 xCO + #.227 xHCHO + #.218 xRCHO + #.008 xMGLY + #.572 xRNO3 + #.85 yR6OOH + #.278 XN + #-.815 XC	1.00e-13			
BP67	IPRD + HV = #1.233 HO2 + #.467 MECO3 + #.3 RCO3 + #1.233 CO + #.3 HCHO + #.467 CCHO + #.233 MEK + #-.233 XC	Phot Set= MACR-06			
<u>Lumped Parameter Organic Products</u>					
BP68	PROD2 + OH = #.472 HO2 + #.473 RO2C + #.070 RO2XC + #.070 zRNO3 + #.002 HCHO + #.001 CCHO + #.143 RCHO + #.329 PROD2 + #.379 xHO2 + #.029 xMECO3 + #.049 xRCO3 + #.211 xHCHO + #.083 xCCHO + #.402 xRCHO + #.115 xMEK + #.007 xPROD2 + #.528 yR6OOH + #.883 XC	1.55e-11			
BP69	PROD2 + HV = #.400 MECO3 + #.600 RCO3 + #1.590 RO2C + #.086 RO2XC + #.086 zRNO3 + #.914 xHO2 + #.303 xHCHO + #.163 xCCHO + #.780 xRCHO + yR6OOH + #-.085 XC	Phot Set= MEK-06, qy= 4.86e-3			

Table A-2 (continued)

Label	Reaction and Products [a]	Rate Parameters [b]			
		k(300)	A	Ea	B
BP70	RNO3 + OH = #.019 NO2 + #.189 HO2 + #.976 RO2C + #.175 RO2XC + #.175 zRNO3 + #.001 RCHO + #.010 MEK + #.007 PROD2 + #.189 RNO3 + #.312 xNO2 + #.305 xHO2 + #.011 xHCHO + #.428 xCCHO + #.036 xRCHO + #.004 xACET + #.170 xMEK + #.030 xPROD2 + #.305 xRNO3 + #.792 yR6OOH + #.175 XN + #.054 XC	7.20e-12			
BP71	RNO3 + HV = NO2 + #.344 HO2 + #.721 RO2C + #.102 RO2XC + #.102 zRNO3 + #.074 HCHO + #.214 CCHO + #.074 RCHO + #.124 MEK + #.190 PROD2 + #.554 xHO2 + #.061 xHCHO + #.230 xCCHO + #.063 xRCHO + #.008 xACET + #.083 xMEK + #.261 xPROD2 + #.656 yR6OOH + #.396 XC				Phot Set= IC3ONO2

Steady-State Peroxy Radical operators (for formation of organic product species formed in peroxy + NO reactions) [c]

PO01	xHCHO = HCHO	k is variable parameter: RO2RO
PO02	xHCHO = XC	k is variable parameter: RO2XRO
PO03	xCCHO = CCHO	k is variable parameter: RO2RO
PO04	xCCHO = #2 XC	k is variable parameter: RO2XRO
PO05	xRCHO = RCHO	k is variable parameter: RO2RO
PO06	xRCHO = #3 XC	k is variable parameter: RO2XRO
PO07	xACET = ACET	k is variable parameter: RO2RO
PO08	xACET = #3 XC	k is variable parameter: RO2XRO
PO09	xMEK = MEK	k is variable parameter: RO2RO
PO10	xMEK = #4 XC	k is variable parameter: RO2XRO
PO11	xPROD2 = PROD2	k is variable parameter: RO2RO
PO12	xPROD2 = #6 XC	k is variable parameter: RO2XRO
PO13	xGLY = GLY	k is variable parameter: RO2RO
PO14	xGLY = #2 XC	k is variable parameter: RO2XRO
PO15	xMGLY = MGLY	k is variable parameter: RO2RO
PO16	xMGLY = #3 XC	k is variable parameter: RO2XRO
PO17	xBACL = BACL	k is variable parameter: RO2RO
PO18	xBACL = #4 XC	k is variable parameter: RO2XRO
PO19	xBALD = BALD	k is variable parameter: RO2RO
PO20	xBALD = #7 XC	k is variable parameter: RO2XRO
PO21	xAFG1 = AFG1	k is variable parameter: RO2RO
PO22	xAFG1 = #5 XC	k is variable parameter: RO2XRO
PO23	xAFG2 = AFG2	k is variable parameter: RO2RO
PO24	xAFG2 = #5 XC	k is variable parameter: RO2XRO
PO25	xAFG3 = AFG3	k is variable parameter: RO2RO
PO26	xAFG3 = #7 XC	k is variable parameter: RO2XRO
PO27	xMACR = MACR	k is variable parameter: RO2RO
PO28	xMACR = #4 XC	k is variable parameter: RO2XRO
PO29	xMVK = MVK	k is variable parameter: RO2RO
PO30	xMVK = #4 XC	k is variable parameter: RO2XRO
PO31	xIPRD = IPRD	k is variable parameter: RO2RO
PO32	xIPRD = #5 XC	k is variable parameter: RO2XRO

Table A-2 (continued)

Label	Reaction and Products [a]	Rate Parameters [b]			
		k(300)	A	Ea	B
PO33	xRNO3 = RNO3	k is variable parameter: RO2RO			
PO34	xRNO3 = #6 XC + XN	k is variable parameter: RO2XRO			
PO35	xHCOOH = HCOOH	k is variable parameter: RO2RO			
PO36	xHCOOH = XC	k is variable parameter: RO2XRO			
PO37	xCCOOH = CCOOH	k is variable parameter: RO2RO			
PO38	xCCOOH = #2 XC	k is variable parameter: RO2XRO			
PO39	xRCOOH = RCOOH	k is variable parameter: RO2RO			
PO40	xRCOOH = #3 XC	k is variable parameter: RO2XRO			
<u>Steady-State Peroxy Radical operators (for formation of organic nitrates formed in peroxy + NO reactions) [d]</u>					
PO41	zRNO3 = RNO3 + #-1 XN	k is variable parameter: RO2NO			
PO42	zRNO3 = PROD2 + HO2	k is variable parameter: RO22NN			
PO43	zRNO3 = #6 XC	k is variable parameter: RO2XRO			
<u>Steady-State Peroxy Radical operators (for formation of hydroperoxides formed in peroxy + HO₂ reactions) [e]</u>					
PO44	yROOH = ROOH + #-3 XC	k is variable parameter: RO2HO2			
PO45	yROOH = MEK + #-4 XC	k is variable parameter: RO2RO2M			
PO46	yROOH =	k is variable parameter: RO2RO			
PO47	yR6OOH = R6OOH + #-6 XC	k is variable parameter: RO2HO2			
PO48	yR6OOH = PROD2 + #-6 XC	k is variable parameter: RO2RO2M			
PO49	yR6OOH =	k is variable parameter: RO2RO			
PO50	yRAOOH = RAOOH + #-8 XC	k is variable parameter: RO2HO2			
PO51	yRAOOH = PROD2 + #-6 XC	k is variable parameter: RO2RO2M			
PO52	yRAOOH =	k is variable parameter: RO2RO			
<u>Explicitly Represented Primary Organics</u>					
BE01	CH4 + OH = H2O + MEO2	6.62e-15	1.85e-12	3.36	
BE02	ETHENE + OH = RO2C + xHO2 + #1.61 xHCHO + #.195 xCCHO + yROOH	8.15e-12	Falloff, F=0.60, N=1.00 0: 1.00e-28 inf: 8.80e-12	0.00 0.00	-4.50 -0.85
BE03	ETHENE + O3 = #.16 OH + #.16 HO2 + #.51 CO + #.12 CO2 + HCHO + #.37 HCOOH	1.68e-18	9.14e-15	5.13	
BE04	ETHENE + NO3 = RO2C + xHO2 + xRCHO + yROOH + #-1 XC + XN	2.24e-16	3.30e-12	5.72	2.00
BE05	ETHENE + O3P = #.8 HO2 + #.51 MEO2 + #.29 RO2C + #.51 CO + #.1 CCHO + #.29 xHO2 + #.278 xCO + #.278 xHCHO + #.012 xGLY + #.29 yROOH + #.2 XC	7.43e-13	1.07e-11	1.59	
BE06	ISOPRENE + OH = #.986 RO2C + #.093 {RO2XC + zRNO3} + #.907 xHO2 + #.624 xHCHO + #.23 xMACR + #.32 xMVK + #.357 xIPRD + yR6OOH + #- 0.167 XC	9.96e-11	2.54e-11	-0.81	
BE07	ISOPRENE + O3 = #.266 OH + #.066 HO2 + #.192 RO2C + #.008 {RO2XC + zRNO3} + #.275 CO + #.122 CO2 + #.4 HCHO + #.1 PROD2 + #.39 MACR + #.16 MVK + #.15 IPRD + #.204 HCOOH + #.192 {xMACO3 + xHCHO} + #.2 yR6OOH + #-0.559 XC	1.34e-17	7.86e-15	3.80	

Table A-2 (continued)

Label	Reaction and Products [a]	Rate Parameters [b]			
		k(300)	A	Ea	B
BE08	ISOPRENE + NO3 = #.936 RO2C + #.064 {RO2XC + zRNO3} + #.749 xHO2 + #.187 xNO2 + #.936 xIPRD + yR6OOH + #-0.064 XC + #.813 XN	6.81e-13	3.03e-12	0.89	
BE09	ISOPRENE + O3P = #.25 MEO2 + #.24 RO2C + #.01 {RO2XC + zRNO3} + #.75 PROD2 + #.24 xMACO3 + #.24 xHCHO + #.25 yR6OOH + #-1.01 XC	3.50e-11			
BE10	ACETYLEN + OH = #.7 OH + #.3 HO2 + #.3 CO + #.7 GLY + #.3 HCOOH	7.56e-13	Falloff, F=0.60, N=1.00		
BE11	ACETYLEN + O3 = #.5 OH + #1.5 HO2 + #1.5 CO + #.5 CO2	1.16e-20	1.00e-14	8.15	
BE12	BENZENE + OH = #.116 OH + #.29 {RO2C + xHO2} + #.024 {RO2XC + zRNO3} + #.57 {HO2 + CRES} + #.116 AFG3 + #.290 xGLY + #.029 xAFG1 + #.261 xAFG2 + #.314 yRAOOH + #-0.976 XC	1.22e-12	2.33e-12	0.38	
<u>Reactions of Compounds represented explicitly in the chamber simulations</u>					
CH05	N-C4 + OH = #1.334 RO2C + #.079 RO2XC + #.079 zRNO3 + #.921 xHO2 + #.632 xCCHO + #.120 xRCHO + #.485 xMEK + yROOH + #-0.038 XC	2.38e-12	1.63e-12	-0.23	
CH07	N-C6 + OH = #1.562 RO2C + #.225 RO2XC + #.225 zRNO3 + #.775 xHO2 + #.011 xCCHO + #.113 xRCHO + #.688 xPROD2 + yR6OOH + #.161 XC	5.25e-12	7.62e-12	0.22	
CH09	N-C8 + OH = #1.432 RO2C + #.354 RO2XC + #.354 zRNO3 + #.646 xHO2 + #.024 xRCHO + #.622 xPROD2 + yR6OOH + #2.072 XC	8.16e-12	2.45e-12	-0.72	
CH11	PROPENE + OH = #.984 RO2C + #.016 RO2XC + #.016 zRNO3 + #.984 xHO2 + #.984 xHCHO + #.984 xCCHO + yROOH + #-0.048 XC	2.60e-11	4.85e-12	-1.00	
CH12	PROPENE + O3 = #.350 OH + #.165 HO2 + #.355 MEO2 + #.525 CO + #.215 CO2 + #.500 HCHO + #.500 CCHO + #.185 HCOOH + #.075 CCOOH + #.070 XC	1.05e-17	5.51e-15	3.73	
CH13	PROPENE + NO3 = #.949 RO2C + #.051 RO2XC + #.051 zRNO3 + #.949 xHO2 + yROOH + #2.694 XC + XN	9.73e-15	4.59e-13	2.30	
CH14	PROPENE + O3P = #.450 RCHO + #.550 MEK + #-0.550 XC	4.01e-12	1.02e-11	0.56	
CH16	T-2-BUTE + OH = #.965 RO2C + #.035 RO2XC + #.035 zRNO3 + #.965 xHO2 + #1.930 xCCHO + yROOH + #-0.070 XC	6.32e-11	1.01e-11	-1.09	
CH17	T-2-BUTE + O3 = #.540 OH + #.170 HO2 + #.710 MEO2 + #.540 CO + #.310 CO2 + CCHO + #.150 CCOOH + #.140 XC	1.95e-16	6.64e-15	2.10	
CH18	T-2-BUTE + NO3 = #.920 RO2C + #.080 RO2XC + #.080 zRNO3 + #.705 xNO2 + #.215 xHO2 + #1.410 xCCHO + #.215 xRNO3 + yROOH + #-0.590 XC + #.080 XN	3.93e-13	1.10e-13	-0.76	
CH19	T-2-BUTE + O3P = MEK	1.99e-11	1.09e-11	-0.36	

Table A-2 (continued)

Label	Reaction and Products [a]	Rate Parameters [b]			
		k(300)	A	Ea	B
CH21	TOLUENE + OH = #.312 {OH + AFG3} + #.181 {HO2 + CRES} + #.454 {RO2C + xHO2} + #.054 {RO2XC + zRNO3} + #.238 xGLY + #.151 xMGLY + #.065 xBALD + #.195 xAFG1 + #.195 xAFG2 + #.073 yR6OOH + #.435 yRAOOH + #-.109 XC	5.58e-12	1.81e-12	-0.67	
CH23	M-XYLENE + OH = #.239 {OH + AFG3} + #.159 {HO2 + CRES} + #.52 {RO2C + xHO2} + #.082 {RO2XC + zRNO3} + #.100 xGLY + #.380 xMGLY + #.041 xBALD + #.336 xAFG1 + #.144 xAFG2 + #.047 yR6OOH + #.555 yRAOOH + #.695 XC	2.31e-11			
<u>Reactions of Lumped Species used in Atmospheric Reactivity Simulations</u>					
BL01	ALK1 + OH = RO2C + xHO2 + xCCHO + yROOH	2.54e-13	1.34e-12	0.99	
BL02	ALK2 + OH = #.965 RO2C + #.035 {RO2XC + zRNO3} + #.965 xHO2 + #.261 xRCHO + #.704 xACET + yROOH + #-.105 XC	1.11e-12	1.49e-12	0.17	
BL03	ALK3 + OH = #1.253 RO2C + #.07 {RO2XC + zRNO3} + #.694 xHO2 + #.236 xTBUO + #.026 xHCHO + #.445 xCCHO + #.122 xRCHO + #.024 xACET + #.332 xMEK + yROOH + #-.046 XC	2.31e-12	1.51e-12	-0.25	
BL04	ALK4 + OH = #1.773 RO2C + #.144 {RO2XC + zRNO3} + #.834 xHO2 + #.011 xMEO2 + #.011 xMECO3 + #.002 xCO + #.030 xHCHO + #.454 xCCHO + #.242 xRCHO + #.442 xACET + #.110 xMEK + #.128 xPROD2 + yR6OOH + #-.097 XC	4.26e-12	3.67e-12	-0.09	
BL05	ALK5 + OH = #1.597 RO2C + #.348 {RO2XC + zRNO3} + #.652 xHO2 + #.037 xHCHO + #.099 xCCHO + #.199 xRCHO + #.066 xACET + #.080 xMEK + #.425 xPROD2 + yR6OOH + #2.012 XC	9.22e-12	2.65e-12	-0.74	
BL06	OLE1 + OH = #1.138 RO2C + #.095 {RO2XC + zRNO3} + #.904 xHO2 + #.001 xMEO2 + #.700 xHCHO + #.301 xCCHO + #.470 xRCHO + #.005 xACET + #.119 xPROD2 + #.026 xMACR + #.008 xMVK + #.006 xIPRD + yROOH + #.822 XC	3.29e-11	6.18e-12	-1.00	
BL07	OLE1 + O3 = #.193 OH + #.116 HO2 + #.104 MEO2 + #.063 RO2C + #.004 {RO2XC + zRNO3} + #.368 CO + #.125 CO2 + #.500 HCHO + #.147 CCHO + #.353 RCHO + #.006 MEK + #.189 PROD2 + #.185 HCOOH + #.022 CCOOH + #.112 RCOOH + #.040 xHO2 + #.007 xCCHO + #.031 xRCHO + #.002 xACET + #.044 yR6OOH + #.69 XC	1.09e-17	3.15e-15	3.38	
BL08	OLE1 + NO3 = #1.312 RO2C + #.176 {RO2XC + zRNO3} + #.824 xHO2 + #.009 xCCHO + #.002 xRCHO + #.024 xACET + #.546 xRNO3 + yR6OOH + #.454 XN + #.572 XC	1.44e-14	4.73e-13	2.08	
BL09	OLE1 + O3P = #.450 RCHO + #.437 MEK + #.113 PROD2 + #1.224 XC	5.02e-12	1.49e-11	0.65	

Table A-2 (continued)

Label	Reaction and Products [a]	Rate Parameters [b]			
		k(300)	A	Ea	B
BL10	OLE2 + OH = #.966 RO2C + #.086 {RO2XC + zRNO3} + #.914 xHO2 + #.209 xHCHO + #.787 xCCHO + #.483 xRCHO + #.136 xACET + #.076 xMEK + #.021 xPROD2 + #.027 xMACR + #.002 xMVK + #.037 xIPRD + yR6OOH + #.113 XC	6.41e-11	1.26e-11	-0.97	
BL11	OLE2 + O3 = #.421 OH + #.093 HO2 + #.290 MEO2 + #.199 RO2C + #.003 {RO2XC + zRNO3} + #.296 CO + #.162 CO2 + #.152 HCHO + #.426 CCHO + #.316 RCHO + #.048 ACET + #.031 MEK + #.042 PROD2 + #.028 MACR + #.021 MVK + #.033 HCOOH + #.061 CCOOH + #.222 RCOOH + #.039 xHO2 + #.147 xMECO3 + #.007 xRCO3 + #.108 xHCHO + #.066 xCCHO + #.019 xRCHO + #.196 yR6OOH + #.133 XC	1.24e-16	8.15e-15	2.49	
BL12	OLE2 + NO3 = #1.185 RO2C + #.136 {RO2XC + zRNO3} + #.409 xNO2 + #.423 xHO2 + #.033 xMEO2 + #.074 xHCHO + #.546 xCCHO + #.153 xRCHO + #.110 xACET + #.002 xMEK + #.026 xMVK + #.007 xIPRD + #.322 xRNO3 + yR6OOH + #.270 XN + #.117 XC	7.70e-13	2.15e-13	-0.76	
BL13	OLE2 + O3P = #.014 HO2 + #.013 RO2C + #.074 RCHO + #.709 MEK + #.203 PROD2 + #.007 xHO2 + #.007 xMACO3 + #.006 xCO + #.006 xMACR + #.014 yR6OOH + #.666 XC	2.06e-11	1.43e-11	-0.22	
BL14	ARO1 + OH = #.283 OH + #.166 HO2 + #.483 RO2C + #.068 {RO2XC + zRNO3} + #.166 CRES + #.283 AFG3 + #.483 xHO2 + #.217 xGLY + #.138 xMGLY + #.049 xBALD + #.079 xPROD2 + #.164 xAFG1 + #.192 xAFG2 + #.150 yR6OOH + #.402 yRAOOH + #.004 XC	6.18e-12			
BL15	ARO2 + OH = #.199 OH + #.108 HO2 + #.582 RO2C + #.111 RO2XC + #.111 zRNO3 + #.108 CRES + #.199 AFG3 + #.582 xHO2 + #.111 xGLY + #.291 xMGLY + #.104 xBACL + #.033 xBALD + #.042 xPROD2 + #.223 xAFG1 + #.211 xAFG2 + #.074 xAFG3 + #.090 yR6OOH + #.603 yRAOOH + #1.503 XC	2.20e-11			
BL16	TERP + OH = #1.147 RO2C + #.2 {RO2XC + zRNO3} + #.759 xHO2 + #.042 xRCO3 + #.002 xCO + #.264 xHCHO + #.533 xRCHO + #.036 xACET + #.005 xMEK + #.255 xPROD2 + #.009 xMGLY + #.014 xBACL + #.002 xMVK + #.001 xIPRD + yR6OOH + #5.055 XC	7.98e-11	1.87e-11	-0.86	

Table A-2 (continued)

Label	Reaction and Products [a]	Rate Parameters [b]			
		k(300)	A	Ea	B
BL17	TERP + O3 = #.585 OH + #.052 HO2 + #.875 RO2C + #.203 RO2XC + #.203 zRNO3 + #.166 CO + #.045 CO2 + #.079 HCHO + #.004 MEK + #.409 PROD2 + #.107 HCOOH + #.043 RCOOH + #.067 xHO2 + #.126 xMECO3 + #.149 xRCO3 + #.019 xCO + #.150 xHCHO + #.220 xRCHO + #.165 xACET + #.001 xGLY + #.002 xMGLY + #.055 xBACL + #.001 xMACR + #.001 xIPRD + #.545 yR6OOH + #3.526 XC	6.99e-17	1.02e-15	1.60	
BL18	TERP + NO3 = #1.508 RO2C + #.397 RO2XC + #.397 zRNO3 + #.422 xNO2 + #.162 xHO2 + #.019 xRCO3 + #.010 xCO + #.017 xHCHO + #.001 xCCHO + #.509 xRCHO + #.174 xACET + #.001 xMGLY + #.003 xMACR + #.001 xMVK + #.002 xIPRD + #.163 xRNO3 + yR6OOH + #4.476 XC + #.415 XN	6.53e-12	1.28e-12	-0.97	
BL19	TERP + O3P = #.147 RCHO + #.853 PROD2 + #4.441 XC	3.71e-11			

[a] Format of reaction listing: “=” separates reactants from products; “#number” indicates stoichiometric coefficient, “#coefficient {product list}” means that the stoichiometric coefficient is applied to all the products listed.

[b] Except as indicated, the rate constants are given by $k(T) = A \cdot (T/300)^B \cdot e^{-E_a/RT}$, where the units of k and A are $\text{cm}^3 \text{ molec}^{-1} \text{ s}^{-1}$, Ea are kcal mol^{-1} , T is $^{\circ}\text{K}$, and $R=0.0019872 \text{ kcal mol}^{-1} \text{ deg}^{-1}$. The following special rate constant expressions are used:

Phot Set = name: The absorption cross sections and (if applicable) quantum yields for the photolysis reaction are given by Carter (2007). Here, “name” indicates the photolysis set used. If a “qy=number” notation is given, the number given is the overall quantum yield, which is assumed to be wavelength independent.

Falloff: The rate constant as a function of temperature and pressure is calculated using $k(T,M) = \{k_0(T) \cdot [M] / [1 + k_0(T) \cdot [M] / k_{inf}(T)]\} \cdot F^Z$, where $Z = \{1 + [\log_{10} \{k_0(T) \cdot [M] / k_{inf}(T)\} / N]^2\}^{-1}$, [M] is the total pressure in molecules cm^{-3} , F and N are as indicated on the table, and the temperature dependences of k0 and kinf are as indicated on the table.

$k = k_0 + k_3 M / (1 + k_3 M / k_2)$: The rate constant as a function of temperature and pressure is calculated using $k(T,M) = k_0(T) + k_3(T) \cdot [M] \cdot (1 + k_3(T) \cdot [M] / k_2(T))$, where [M] is the total bath gas (air) concentration in molecules cm^{-3} , and the temperature dependences for k0, k2 and k3 are as indicated on the table.

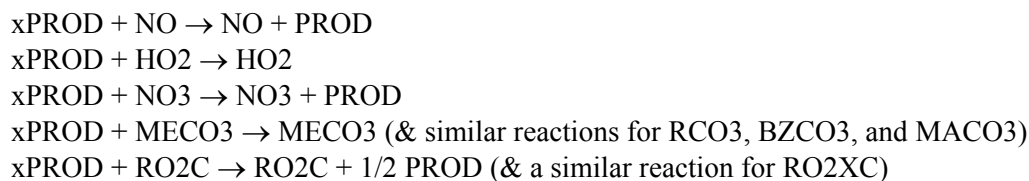
$k = k_1 + k_2 [M]$: The rate constant as a function of temperature and pressure is calculated using $k(T,M) = k_1(T) + k_2(T) \cdot [M]$, where [M] is the total bath gas (air) concentration in molecules cm^{-3} , and the temperature dependences for k1, and k2 are as indicated on the table.

Same K as Rxn xx: Uses the same rate constant as the reaction in the base mechanism with the same label.

[c] The xPROD chemical operator species are used to represent the formation of radicals and products from alkoxy radicals formed in the reactions of peroxy radicals with NO, NO₃, and other peroxy radicals. These products are not formed when peroxy radicals react with HO₂ and acyl peroxy radicals, since those reactions are assumed not form alkoxy radicals, but instead form hydroperoxides or H-shift disproportion products that are represented by separate yROOH chemical operator species, discussed in a separate footnote. The reactions of peroxy radicals with other peroxy

Table A-2 (continued)

radicals are assumed to form alkoxy radicals 50% of the time, so the products from alkoxy radical reactions are represented as being formed in 50% yields in these reactions. The consumption and products formed from these species can be represented in several ways. The most straightforward method is to include a reaction for each of the types of peroxy radical reactions, as follows:

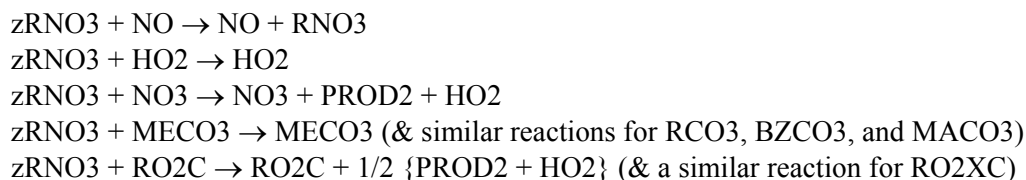


where "PROD" represents the product species for the operator (e.g, HO₂ for xHO₂). The rate constants for these reactions should be the same as the rate constant for the corresponding reactions of RO₂C or RO₂XC. This is a somewhat cumbersome method because it requires 9 reactions for each of the many xPROD species. An alternative method, implemented in this table, uses the coefficient "RO₂RO" to determine the rate of formation of the product species and "RO₂XRO" to represent processes where the product is not formed. These are calculated as follows, where the k(RO₂+.)'s refer to the rate constants for the reactions of RO₂C or RO₂XC with the indicated reactant.

$$\begin{aligned} \text{RO}_2\text{RO} &= k(\text{RO}_2+\text{NO})[\text{NO}] + k(\text{RO}_2+\text{NO}_3)[\text{NO}_3] + 0.5 k(\text{RO}_2+\text{MEO}_2)[\text{MEO}_2] + \\ &\quad 0.5 k(\text{RO}_2+\text{RO}_2)\{[\text{RO}_2\text{C}]+[\text{RO}_2\text{XC}]\} \\ \text{RO}_2\text{XRO} &= k(\text{RO}_2+\text{HO}_2)[\text{HO}_2] + k(\text{RO}_2+\text{MECO}_3)\{[\text{MECO}_3]+[\text{RCO}_3]+[\text{BZCO}_3]+ \\ &\quad [\text{MACO}_3]\} + 0.5 k(\text{RO}_2+\text{MEO}_2)[\text{MEO}_2] + 0.5 k(\text{RO}_2+\text{RO}_2)\{[\text{RO}_2\text{C}]+ [\text{RO}_2\text{XC}]\} \end{aligned}$$

The steady state approximation must be used for these operators when this representation is used, and the operators must not be allowed to be diluted or transported.

- [d] The zRNO₃ chemical operator species is used to represent the formation organic nitrates formed when peroxy radicals react with NO, or formation of radicals and products from alkoxy radicals formed in the reactions of peroxy radicals with NO₃ and other peroxy radicals. These products are not formed when peroxy radicals react with HO₂ and acyl peroxy radicals, since those reactions are assumed not form organic nitrates or alkoxy radicals, but instead form hydroperoxides or H-shift disproportionation products that are represented by separate yROOH chemical operator species, discussed in a separate footnote. At present the mechanism has only one zRNO₃ operator to correspond to the single lumped organic nitrate model species, but other such operators can be added if it is desired to have separate organic nitrate model species, such as, for example, those to represent semi-volatile organic nitrates that may contribute to SOA. In the case of zRNO₃, the products resulting if alkoxy radicals are formed in the RCO₃ or RO₂ reactions would depend on reactant and individual radicals, and are approximated by PROD₂ and HO₂ (as might occur following the reaction of a peroxy radical with O₂ to form HO₂ and a ketone species). As with the xPROD species, the consumption and products formed from these species can be represented in several ways, with the most straightforward method being to include a reaction for each of the types of peroxy radical reactions, as follows:



The rate constants for these reactions should be the same as the rate constant for the corresponding reactions of RO₂C or RO₂XC. As with xPROD, an alternative method, requiring fewer reactions, is implemented in this table. In this case, the coefficient "RO₂NO" is used to determine the rate of formation of organic nitrates, "RO₂NN" is used to determine the rate of formation of the alkoxy

Table A-2 (continued)

radical products, and "RO2XRO" is used to represent processes where these products are not formed, and is the same as used for xPROD. These are calculated as follows, where the k(RO2+..)'s refer to the rate constants for the reactions of RO2C or RO2XC with the indicated reactant.

$$\text{RO2NO} = k(\text{RO2+NO})[\text{NO}]$$

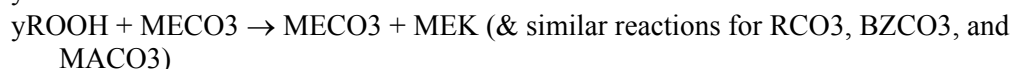
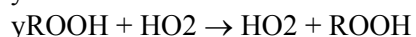
$$\text{RO22NN} = k(\text{RO2+NO3})[\text{NO3}] + 0.5 k(\text{RO2+MEO2})[\text{MEO2}] + 0.5 k(\text{RO2+RO2})\{[\text{RO2C}] + [\text{RO2XC}]\}$$

$$\text{RO2XRO} = k(\text{RO2+HO2})[\text{HO2}] + k(\text{RO2+MECO3})\{[\text{MECO3}] + [\text{RCO3}] + [\text{BZCO3}] + [\text{MACO3}]\} + 0.5 k(\text{RO2+MEO2})[\text{MEO2}] + 0.5 k(\text{RO2+RO2})\{[\text{RO2C}] + [\text{RO2XC}]\}$$

(same as used for xPROD)

The steady state approximation must be used for these operators when this representation is used, and the operators must not be allowed to be diluted or transported.

- [e] The yROOH chemical operator species is used to represent the formation of organic hydroperoxides formed with peroxy radicals react with HO₂, or of H-shift disproportionation products formed when peroxy radicals react with acyl peroxy radicals or (in 50% yields) with other peroxy radicals. Note that the products formed when peroxy radicals react to form alkoxy radicals or organic nitrates (in the NO reaction) are represented using separate xPROD or zRNO3 species, and together these three types of operators represent all the products and radicals formed. Separate such yROOH species are used to represent formation of hydroperoxides or H-shift disproportion products in different molecular weight ranges or volatilities, and more can be added as needed for appropriate predictions of SOA formation. The hydroperoxide formed in the HO₂ reaction is represented by either ROOH, R6OOH, or RAOOH, and the H-shift disproportion products are represented by either MEK (for yROOH) or PROD2 (for the others). As with the xPROD and zRNO3 species, the consumption and products formed from these species can be represented in several ways, with the most straightforward method being to include a reaction for each of the types of peroxy radical reactions, as follows for yROOH (the reactions for the other two are analogous).



The rate constants for these reactions should be the same as the rate constant for the corresponding reactions of RO2C or RO2XC. As with the other operators, an alternative method, requiring fewer reactions, is implemented in this table. In this case, the coefficient "RO2HO2" is used to determine the rate of formation of organic hydroperoxides, "RO2RO2M" to determine the rate of formation of H-shift disproportion products, and "RO2RO" is used to represent processes where these products are not formed. Note that the latter is the same as the coefficient that is used to represent the formation products from the xPROD species. These are calculated as follows, where the k(RO2+..)'s refer to the rate constants for the reactions of RO2C or RO2XC with the indicated reactant.

$$\text{RO2HO2} = k(\text{RO2+HO2})[\text{HO2}]$$

$$\text{RO2RO2M} = k(\text{RO2+MECO3})\{[\text{MECO3}] + [\text{RCO3}] + [\text{BZCO3}] + [\text{MACO3}]\} + 0.5 k(\text{RO2+MEO2})[\text{MEO2}] + 0.5 k(\text{RO2+RO2})\{[\text{RO2C}] + [\text{RO2XC}]\}$$

$$\text{RO2RO} = k(\text{RO2+NO})[\text{NO}] + k(\text{RO2+NO3})[\text{NO3}] + 0.5 k(\text{RO2+MEO2})[\text{MEO2}] + 0.5 k(\text{RO2+RO2})\{[\text{RO2C}] + [\text{RO2XC}]\}$$

The steady state approximation must be used for these operators when this representation is used, and the operators must not be allowed to be diluted or transported.

Table A-3. Summary of photolysis rates used in chamber and ambient simulations. Absorption cross sections and quantum yields used to calculate these photolysis rates are given by Carter (2007) for reactions in the base mechanism and in Table 4 for those in the methyl iodide mechanism.

Phot File	Chamber [a]	Photolysis rates (min ⁻¹)									
		Ambient simulations (as function of solar zenith angle) [b]									
		Z=0	Z=10	Z=20	Z=30	Z=40	Z=50	Z=60	Z=70	Z=78	Z=86
<u>Base Mechanism</u>											
NO2-06	0.130	0.723	0.718	0.702	0.676	0.631	0.560	0.430	0.253	0.093	0.005
NO3NO-06	2.76e-4	1.91e+0	1.91e+0	1.90e+0	1.89e+0	1.87e+0	1.82e+0	1.65e+0	1.37e+0	9.15e-1	4.85e-1
NO3NO2-6	5.46e-2	1.54e+1	1.54e+1	1.53e+1	1.52e+1	1.49e+1	1.44e+1	1.29e+1	1.03e+1	6.50e+0	2.80e+0
O3O1D-06	2.07e-4	3.06e-3	2.96e-3	2.68e-3	2.24e-3	1.67e-3	1.06e-3	4.91e-4	1.33e-4	2.01e-5	3.66e-7
O3O3P-06	5.47e-4	3.66e-2	3.66e-2	3.62e-2	3.57e-2	3.48e-2	3.32e-2	2.95e-2	2.37e-2	1.57e-2	8.36e-3
HONO-06	3.17e-2	1.14e-1	1.13e-1	1.10e-1	1.06e-1	9.78e-2	8.54e-2	6.38e-2	3.55e-2	1.18e-2	4.32e-4
HNO3	4.99e-6	5.40e-5	5.28e-5	4.91e-5	4.31e-5	3.49e-5	2.50e-5	1.40e-5	4.99e-6	9.91e-7	2.29e-8
HNO4-06	7.53e-5	5.42e-4	5.32e-4	5.01e-4	4.52e-4	3.81e-4	2.90e-4	1.77e-4	7.28e-5	1.70e-5	4.56e-7
H2O2	1.02e-4	5.64e-4	5.56e-4	5.29e-4	4.86e-4	4.21e-4	3.33e-4	2.14e-4	9.43e-5	2.35e-5	6.64e-7
PAN	8.11e-6	6.12e-5	6.00e-5	5.65e-5	5.08e-5	4.26e-5	3.22e-5	1.95e-5	7.90e-6	1.81e-6	4.80e-8
HCHOR-06	2.86e-4	2.76e-3	2.72e-3	2.59e-3	2.36e-3	2.03e-3	1.58e-3	9.85e-4	4.05e-4	9.08e-5	2.35e-6
HCHOM-06	6.92e-4	3.12e-3	3.08e-3	2.97e-3	2.77e-3	2.47e-3	2.02e-3	1.37e-3	6.41e-4	1.69e-4	5.00e-6
CCHO_R	2.86e-5	4.16e-4	4.06e-4	3.75e-4	3.27e-4	2.60e-4	1.81e-4	9.50e-5	2.99e-5	4.86e-6	8.30e-8
C2CHO	1.19e-4	1.40e-3	1.37e-3	1.28e-3	1.14e-3	9.29e-4	6.74e-4	3.80e-4	1.36e-4	2.62e-5	5.79e-7
ACET-06	4.36e-6	6.47e-5	6.28e-5	5.69e-5	4.78e-5	3.60e-5	2.32e-5	1.10e-5	3.05e-6	4.50e-7	7.35e-9
MEK-06	7.87e-5	9.66e-4	9.45e-4	8.80e-4	7.78e-4	6.33e-4	4.56e-4	2.54e-4	8.86e-5	1.66e-5	3.53e-7
COOH	8.03e-5	3.94e-4	3.89e-4	3.71e-4	3.42e-4	2.99e-4	2.40e-4	1.58e-4	7.21e-5	1.89e-5	5.51e-7
GLY-07R	1.08e-3	9.06e-3	9.00e-3	8.78e-3	8.44e-3	7.86e-3	6.97e-3	5.39e-3	3.29e-3	1.35e-3	1.31e-4
GLY-07M	4.98e-4	3.18e-3	3.14e-3	3.00e-3	2.78e-3	2.44e-3	1.98e-3	1.33e-3	6.41e-4	1.91e-4	8.80e-6
MGLY-06	1.15e-3	1.56e-2	1.56e-2	1.52e-2	1.47e-2	1.38e-2	1.24e-2	9.83e-3	6.27e-3	2.72e-3	2.87e-4
BACL-07	2.33e-3	2.67e-2	2.66e-2	2.61e-2	2.54e-2	2.40e-2	2.18e-2	1.75e-2	1.12e-2	4.81e-3	4.67e-4
BALD-06	1.49e-2	5.10e-2	5.05e-2	4.88e-2	4.61e-2	4.17e-2	3.52e-2	2.49e-2	1.26e-2	3.71e-3	1.17e-4
AFG1	7.71e-2	3.87e-1	3.83e-1	3.70e-1	3.50e-1	3.17e-1	2.69e-1	1.94e-1	1.04e-1	3.51e-2	1.99e-3
MACR-06	3.88e-5	1.97e-4	1.94e-4	1.86e-4	1.72e-4	1.51e-4	1.21e-4	7.98e-5	3.64e-5	9.42e-6	2.74e-7
MVK-06	1.49e-5	7.50e-5	7.40e-5	7.07e-5	6.54e-5	5.73e-5	4.60e-5	3.02e-5	1.37e-5	3.51e-6	1.01e-7
IC3ONO2	2.06e-5	2.35e-4	2.30e-4	2.15e-4	1.91e-4	1.57e-4	1.15e-4	6.57e-5	2.41e-5	4.80e-6	1.11e-7
<u>Methyl Iodide Mechanism</u>											
CH3I	5.95e-5	5.17e-4	5.06e-4	4.74e-4	4.22e-4	3.50e-4	2.59e-4	1.53e-4	5.93e-5	1.30e-5	3.29e-7
BRNO2	4.65e-2	4.07e-1	4.05e-1	3.97e-1	3.85e-1	3.64e-1	3.30e-1	2.63e-1	1.68e-1	7.32e-2	8.42e-3
HI	1.00e-4	8.87e-4	8.71e-4	8.19e-4	7.36e-4	6.16e-4	4.64e-4	2.77e-4	1.09e-4	2.39e-5	6.07e-7
HOI	8.48e-1	7.28e+0	7.25e+0	7.11e+0	6.89e+0	6.51e+0	5.88e+0	4.67e+0	2.96e+0	1.26e+0	1.29e-1
BRONO2	1.82e-2	1.11e-1	1.10e-1	1.07e-1	1.03e-1	9.56e-2	8.44e-2	6.48e-2	3.92e-2	1.60e-2	1.90e-3

[a] Photolysis rates for a chamber experiment with blacklight light source. The NO₂ photolysis rate is for run EPA736. For runs with a different NO₂ photolysis rate, multiply all photolysis rates by the same factor to get the appropriate NO₂ photolysis rate. See Figure 3 for the NO₂ photolysis rate as a function of run number.

[b] See Carter (1994) for documentation of solar actinic fluxes used in the atmospheric reactivity calculations.